

# UNDERSTANDING AND IMPROVING HYPERBOLIC DEEP REINFORCEMENT LEARNING

Timo Klein<sup>\*,1,2</sup>, Thomas Lang<sup>\*,1,2</sup>, Andrii Shkabrii<sup>1,2</sup>, Alexander Sturm<sup>1,2</sup>, Kevin Sidak<sup>1,2</sup>  
 Lukas Miklautz<sup>3</sup>, Claudia Plant<sup>1,4</sup>, Yllka Velaj<sup>1,4</sup>, Sebastian Tschiatschek<sup>1,4</sup>

<sup>1</sup> Faculty of Computer Science, University of Vienna, Vienna, Austria

<sup>2</sup> Doctoral School Computer Science, University of Vienna, Vienna, Austria

<sup>3</sup> Department of Machine Learning and Systems Biology, Max Planck Institute of Biochemistry, Martinsried, Germany

<sup>4</sup> ds:UniVie, University of Vienna, Vienna, Austria

\* Joint first authors

firstname.lastname@univie.ac.at

## ABSTRACT

The performance of reinforcement learning (RL) agents depends critically on the quality of the underlying feature representations. Hyperbolic feature spaces are well-suited for this purpose, as they naturally capture hierarchical and relational structure often present in complex RL environments. However, leveraging these spaces commonly faces optimization challenges due to the nonstationarity of RL. In this work, we identify key factors that determine the success and failure of training hyperbolic deep RL agents. By analyzing the gradients of core operations in the Poincaré Ball and Hyperboloid models of hyperbolic geometry, we show that large-norm embeddings destabilize gradient-based training, leading to trust-region violations in proximal policy optimization (PPO). Based on these insights, we introduce HYPER++, a new hyperbolic PPO agent that consists of three components: (i) stable critic training through a categorical value loss instead of regression; (ii) feature regularization guaranteeing bounded norms while avoiding the curse of dimensionality from clipping; and (iii) using a more optimization-friendly formulation of hyperbolic network layers. In experiments on ProcGen, we show that HYPER++ guarantees stable learning, outperforms prior hyperbolic agents, and reduces wall-clock time by approximately 30%. On Atari-5 with Double DQN, HYPER++ strongly outperforms Euclidean and hyperbolic baselines. **We release our code at <https://github.com/Probabilistic-and-Interactive-ML/hyper-rl>.**

## 1 INTRODUCTION

Consider a chess-playing agent facing a difficult moment in its game. As it maps out future scenarios, these unfold into a tree of possible future states. Each action commits to one branch and rules out others, and the number of reachable positions grows exponentially with depth. Playing chess can thus be viewed as traversing this expanding tree of possible states. The same structure appears in other sequential decision-making benchmarks such as ProcGen BIGFISH (Cobbe et al., 2020). Here, the agent grows by eating smaller fish, and growth cannot be undone, inducing a natural order. In both cases, the data are inherently hierarchical: each state depends on its predecessors, and future states branch from the present one.

Tree-structured data from sequential decision problems like chess or BIGFISH cannot be embedded in Euclidean space without large distortion: Euclidean volume grows only *polynomially* in radius, whereas tree size grows *exponentially*

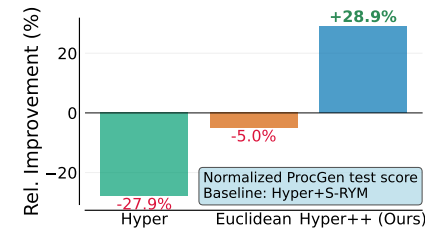


Figure 1: **Baseline improvement on ProcGen.** We compare mean test rewards for our agent (HYPER++), a Euclidean agent, and an unregularized hyperbolic agent (Hyper) with Cetin et al. (2023)’s agent (Hyper+S-RYM).

(Sarkar, 2011; Gromov, 1987). This creates a mismatch between the hierarchical data produced by decision-making agents and the Euclidean representations used by modern deep networks (Cetin et al., 2023). We hypothesize that this mismatch contributes to the data-inefficiency and deployment challenges of deep RL despite impressive successes (Silver et al., 2016; Schriftwieser et al., 2020; Ouyang et al., 2022). But what if there were representations that better match the geometry of sequential decision making?

Hyperbolic geometry (Bolyai, 1896; Lobachevskiĭ, 1891) offers an appealing solution to the limitations of Euclidean representations: Unlike Euclidean space, its exponential volume growth makes it a natural fit for embedding hierarchical data. Since its inception, hyperbolic deep learning has achieved strong results in classification (Ganea et al., 2018), graph learning (Chami et al., 2019), unsupervised representation learning (Mathieu et al., 2019), deep metric learning (Ermolov et al., 2022), and image-text alignment (Pal et al., 2025). Despite its conceptual appeal, the broader adoption has been hampered by significant optimization challenges (Guo et al., 2022; Mishne et al., 2023).

Thus, while hyperbolic geometry is inherently well-suited for RL, its broader adoption in deep RL hinges on a thorough understanding of the associated optimization challenges and potential failure modes. To this end, we study the heuristic trust-region algorithm proximal policy optimization (PPO) with a hybrid Euclidean–hyperbolic encoder, which is a commonly used architecture for Deep RL (Cetin et al., 2023; Salehmoamed et al., 2023). Despite the trust region, hyperbolic PPO agents face **policy-learning issues from unstable encoder gradients**, further amplified by nonstationary data and targets in deep RL (Cetin et al., 2023).

In this paper, we take a step towards a more principled understanding of the underlying optimization issues in hyperbolic deep RL. We start by analyzing key derivatives of mathematical operations of hyperbolic deep learning, which we link to trust-region issues of hyperbolic PPO. We show that neither the Poincaré Ball nor the Hyperboloid —common models for hyperbolic geometry— is immune to gradient instability. Grounded in this analysis, we propose a principled regularization approach to stabilize the training of hyperbolic agents. The resulting agent, **HYPER++**, ensures stable learning by pairing Euclidean feature regularization on the Hyperboloid with a categorical value loss to handle target nonstationarity. HYPER++ improves PPO’s performance and wall-clock time on ProcGen (Figure 1) by approximately 30% over existing hyperbolic agents. We further show that our regularization approach generalizes beyond on-policy methods: applying the same ideas to DDQN (van Hasselt et al., 2016) and the Atari-3 benchmark (Aitchison et al., 2023) also yields strong performance improvements. Our code will be made available.

### Our Key Contributions

1. **Characterization of training issues.** For both the Poincaré Ball and Hyperboloid, we derive gradients of key operations and link them to training instability in deep RL.
2. **Principled regularization.** We study the weaknesses of current approaches and propose improvements rooted in our insights into hyperbolic deep RL training.
3. **HYPER++, a strong hyperbolic agent with stable training.** We integrate a categorical value loss, RMSNorm, and a novel scaling layer for the Hyperboloid model.

## 2 BACKGROUND

This section first reviews Markov decision processes (MDPs) and the PPO optimization procedure (Section 2.1), then presents the mathematical foundations of hyperbolic representation learning in Section 2.2. A more thorough overview of the Poincaré Ball and Hyperboloid models can be found in Ganea et al. (2018); Shimizu et al. (2021); Bdeir et al. (2024).

### 2.1 REINFORCEMENT LEARNING

We formalize RL as a discrete MDP  $M = \langle \mathcal{S}, \mathcal{A}, \mathcal{P}, \mathcal{R}, \gamma \rangle$  with state space  $\mathcal{S}$  and action space  $\mathcal{A}$ . At each time step  $t$ , the agent observes a state  $s \in \mathcal{S}$  and selects an action  $a \in \mathcal{A}$  with its policy  $\pi: \mathcal{S} \rightarrow [0, 1]^{|\mathcal{A}|}$ . The environment generates a reward via its reward function  $\mathcal{R}: \mathcal{S} \times \mathcal{A} \rightarrow \mathbb{R}$  and transitions to the next state according to the transition kernel  $\mathcal{P}: \mathcal{S} \times \mathcal{S} \times \mathcal{A} \rightarrow [0, 1]$ . The agent maximizes discounted future rewards  $J(\pi) = \mathbb{E}_\pi [\sum_{t=0}^{\infty} \gamma^t r(s_t, a_t) \mid \pi]$ , where  $\gamma \in [0, 1]$  is a discount factor determining how much the agent values future rewards (Sutton & Barto, 2018).

---

**PPO** Proximal Policy Optimization (PPO) (Schulman et al., 2017) is an actor-critic algorithm directly maximizing cumulative reward via gradient ascent on a surrogate objective. It replaces the hard trust-region constraint of Trust-Region Policy Optimization (TRPO) (Schulman et al., 2015) with the clipped objective

$$J^{\text{CLIP}}(\theta) = \hat{\mathbb{E}}_t \left[ \min(r_t(\theta)A_t, \text{clamp}(r_t(\theta), 1 - \epsilon, 1 + \epsilon) A_t) \right], \quad (1)$$

where  $r_t(\theta) = \frac{\pi_\theta(a_t|s_t)}{\pi_{\theta_{\text{old}}}(a_t|s_t)}$  are importance sampling ratios of policies parameterized by  $\theta$ , and  $\hat{\mathbb{E}}_t$  is the empirical mean with respect to the samples generated in episode  $t$ . The min-clamping in Equation 1 truncates the incentive to move probability ratios beyond  $[1 - \epsilon, 1 + \epsilon]$ , acting as an unconstrained proxy for TRPO’s KL-divergence trust region (see Appendix B.1).

## 2.2 HYPERBOLIC REPRESENTATION LEARNING

**Hyperbolic Geometry** In this work, we employ two common models of hyperbolic space: the *Poincaré Ball* and the *Hyperboloid*. The two isometrically equivalent (distance-preserving) models are  $d$ -dimensional simply-connected Riemannian submanifolds  $(\mathcal{M}, g)$  with constant negative sectional curvature  $-c$  (see Figure 4), with  $c \in \mathbb{R}_{>0}$ .

**Poincaré Ball** The  $d$ -dimensional *Poincaré Ball* is defined as the Riemannian submanifold  $(\mathbb{P}_c^d, g_{\mathbb{P}_c^d})$ , with  $\mathbb{P}_c^d = \{(x_1, \dots, x_d) \in \mathbb{R}^d : \|x\|^2 < \frac{1}{c}\}$ . Its Riemannian metric  $g_{\mathbb{P}_c^d}$  is given by the collection of inner products  $\langle u, v \rangle_x : \mathcal{T}_x \mathbb{P}_c^d \times \mathcal{T}_x \mathbb{P}_c^d \rightarrow \mathbb{R}$ ,  $(u, v) \mapsto \lambda_x^c \langle u, v \rangle$  that smoothly varies between tangent spaces  $\mathcal{T}_x \mathbb{P}_c^d$  with base points  $x \in \mathbb{P}_c^d$ . That is, the Poincaré Ball is conformal (angle-preserving) to the Euclidean space with conformal factor  $\lambda_x^c = \frac{2}{1 - c \|x\|^2}$ .

**Hyperboloid** The  $d$ -dimensional *Hyperboloid*, often called *Lorentz manifold*, is defined as the forward sheet  $(\mathbb{H}_c^d, g_{\mathbb{H}_c^d})$  of a two-sheeted Hyperboloid, where  $\mathbb{H}_c^d = \{(x_0, \dots, x_d) \in \mathbb{R}^{d+1} : \langle x, x \rangle_{\mathcal{L}} = -\frac{1}{c}, x_0 > 0\}$  and  $\langle x, x \rangle_{\mathcal{L}} = -x_0^2 + x_1^2 + \dots + x_d^2$  is the Minkowski inner product. It is endowed with the Riemannian metric  $g_{\mathbb{H}_c^d}$  that arises when restricting the Minkowski inner product to the tangent spaces  $\mathcal{T}_x \mathbb{H}_c^d$ , i.e.  $\langle u, v \rangle_x : \mathcal{T}_x \mathbb{H}_c^d \times \mathcal{T}_x \mathbb{H}_c^d \rightarrow \mathbb{R}$ ,  $(u, v) \mapsto \langle u, v \rangle_{\mathcal{L}}$ . In this work, we frequently refer to the first component  $x_0$  of  $x \in \mathbb{H}_c^d$  as *time component* and to the other components  $x_{1:d}$  as *space component*.

**Hyperbolic Encoding** In our experiments, we retrieve hyperbolic latent representations by first mapping Euclidean vectors  $v \in \mathbb{R}^d$  to the tangent space at the manifold’s origin  $\bar{0}$ , followed by applying the *exponential map* at the origin  $\exp_{\bar{0}}$ , to project it onto the manifold  $\mathcal{M}$ . This process can be summarized as  $\mathbb{R}^d \xrightarrow{\phi} \mathcal{T}_{\bar{0}} \mathcal{M} \xrightarrow{\exp_{\bar{0}}} \mathcal{M}$ . The *exponential map* at the origin  $\exp_{\bar{0}} : \mathcal{T}_{\bar{0}} \mathcal{M} \rightarrow \mathcal{M}$  maps vectors  $v \in \mathcal{T}_{\bar{0}} \mathcal{M}$  to the manifold  $\mathcal{M}$  such that the curve  $t \in [0, 1] \mapsto \exp_{\bar{0}}(tv)$  is a geodesic (shortest path) joining the manifold’s origin  $\bar{0}$  and  $\exp_{\bar{0}}(v)$ . The specific mapping functions are:

- **Poincaré Ball:** The origin  $\bar{0}$  is the Euclidean origin  $0$ , i.e.  $\phi$  is the identity function and the exponential map at the origin is  $\exp_{\bar{0}} : v \mapsto \frac{\tanh(\sqrt{c} \|v\|)}{\sqrt{c} \|v\|} v$ .
- **Hyperboloid:** The origin is  $\bar{0} = (1/\sqrt{c}, 0, \dots, 0)$ . The map  $\phi$  projects a Euclidean vector  $v \in \mathbb{R}^d$  onto the tangent space  $\mathcal{T}_{\bar{0}} \mathbb{H}_c^d = \{v \in \mathbb{R}^{d+1} : \langle v, \bar{0} \rangle_{\mathcal{L}} = 0\}$  by setting its first coordinate to zero, i.e.  $\phi : v \mapsto (0, v)$ . The exponential map at the origin is  $\exp_{\bar{0}} : v \mapsto \cosh(\sqrt{c} \langle v, v \rangle_{\mathcal{L}}) \bar{0} + \sinh(\sqrt{c} \langle v, v \rangle_{\mathcal{L}}) \frac{v}{\sqrt{c} \langle v, v \rangle_{\mathcal{L}}}$ .

**Hyperbolic Multinomial Logistic Regression** For the policy and value function of our PPO agent, we compute the Multinomial Logistic Regression (MLR) (Lebanon & Lafferty, 2004; Shimizu et al., 2021; Bdeir et al., 2024) in hyperbolic space. The method computes the probability  $p(y = k | x)$  of an input  $x \in \mathcal{M} \simeq \mathbb{R}^d$  belonging to a specific class  $k \in \{1, \dots, K\}$ :

$$p(y = k | x) \propto \exp(v_{z_k, r_k}(x)), \quad v_{z_k, r_k}(x) = \|z_k\|_{\mathcal{T}_{p_k} \mathcal{M}} d_{\mathcal{M}}(x, \mathcal{H}_{z_k, r_k}). \quad (2)$$

Here,  $\exp(v_{z_k, r_k}(x))$  is the logit for class  $k$  and  $v_{z_k, r_k}(x)$  the signed distance to the margin hyperplane  $\mathcal{H}_{z_k, r_k}$  with learnable parameters  $z_k \in \mathbb{R}^d$ ,  $r_k \in \mathbb{R}$  specifying the normal and shift vector  $p_k$ , respectively. The specific definitions for these parameters and the hyperplane itself depend on the hyperbolic model. We expand on this further in Appendix B.3.

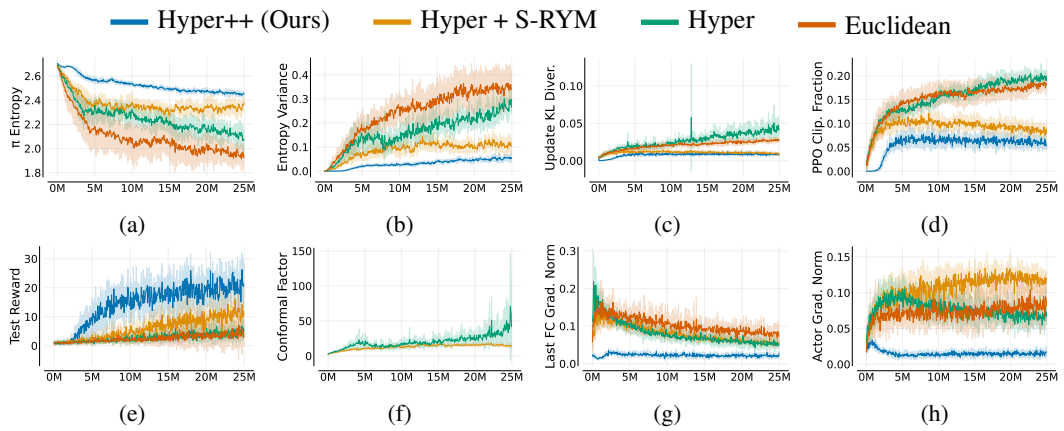


Figure 2: **PPO training metrics.** Unregularized agents (Hyper, Euclidean) lose entropy and show unstable updates (higher update KL and clip fraction), with lower returns and larger gradients (BigFish). Hyper’s conformal factor explodes. In contrast, HYPER++ uses the Hyperboloid, which has no conformal factor. Metrics are means over six seeds with one standard deviation.

### 3 DIAGNOSING ISSUES WITH HYPERBOLIC PPO AGENTS

In this section, we analyze training issues of hyperbolic PPO agents (Section 3.1). We link these issues to the gradients of common hybrid neural network architectures as used in Cetin et al. (2023) in Sections 3.2, 3.3, and 3.4. These networks consist of a shared Euclidean encoder with only the last layers for the actor and the critic being hyperbolic (cf. Figure 11 in the Appendix). Appendices B.3, B.3.1, and B.3.2 contain additional background on the MLR formulations of the Poincaré Ball and the Hyperboloid.

#### 3.1 PPO OPTIMIZATION

PPO’s clipped surrogate objective (Eq. 1) restricts the per-sample importance sampling ratios and acts as a heuristic trust region (Schulman et al., 2017). A high clipping fraction indicates many samples are at the trust region boundary. Crucially, PPO constrains ratios only on the sampled states in a batch. Gradient steps leading to large policy changes on unseen states remain unconstrained, so the heuristic trust region can fail. This cross-state interference can produce large unintended policy shifts beyond the sampled states in the batch (Moalla et al., 2024).

Figure 2 shows key training metrics for hyperbolic PPO training in the BIGFISH environment (top row). As noted by Cetin et al. (2023), unregularized hyperbolic PPO is prone to early entropy collapse in Plot 2a. This coincides with a rapid rise in entropy variance across batch states, producing large policy updates that potentially interfere (Figure 2b). Figures 2c and 2d confirm: unregularized agents experience larger update KL-divergence and more trust-region violations. Cetin et al. (2023) propose to mitigate this with S-RYM, a combination of Euclidean embeddings scaled by  $1/\sqrt{a}$  and SpectralNorm to bound the encoder’s Lipschitz constant (Hyper+S-RYM in Fig. 2). In comparison, our method (Section 4) achieves lower update KL and markedly less clipping while avoiding the overhead of SpectralNorm and instabilities from the conformal factor.

#### 3.2 GRADIENT ANALYSIS PRELIMINARIES

To explain the trust-region instability of the hyperbolic agent, we follow Cetin et al. (2023) and analyze the gradients of the last encoder layer (Fig. 2g). Figure 2f shows that the conformal factor of the Poincaré Ball  $\lambda_x^c = \frac{2}{1-c\|\mathbf{x}\|^2}$  is a key driver for inducing instability. In the following, we derive closed-form, curvature-aware gradients for core hyperbolic layers and maps to study optimization failure points, extending Guo et al. (2022); Mishne et al. (2023) with new expressions for PPO. Below,

we present the gradient with respect to the last Euclidean layer weights  $\mathbf{W}^E$  for a generic loss  $L$ .

$$\frac{\partial L}{\partial \mathbf{W}^E} = \frac{\partial L}{\partial v_{\mathbf{z},r}(\mathbf{x}_H)} \frac{\partial v_{\mathbf{z},r}(\mathbf{x}_H)}{\partial \mathbf{x}_H} \frac{\partial \mathbf{x}_H}{\partial \mathbf{x}_E} \frac{\partial \mathbf{x}_E}{\partial \mathbf{W}^E}, \quad (3)$$

where  $v_{\mathbf{z},r}$  denotes the score function of any hyperbolic multinomial regression (MLR) layer,  $\mathbf{x}_E$  are the Euclidean embeddings from the encoder, and  $\mathbf{x}_H = \exp_{\bar{0}}(\mathbf{x}_E)$  are the embeddings represented as tangent vectors mapped to hyperbolic space. For the Poincaré MLR layer used by Cetin et al. (2023), Guo et al. (2022) have shown that backpropagating through the exponential map yields vanishing gradients near the boundary because the Riemannian gradient scales with the inverse conformal factor gradient:

$$\nabla_{\mathbf{x}_H} \lambda_{\mathbf{x}_H}^c = \frac{4c \mathbf{x}_H}{(1 - c\|\mathbf{x}_H\|^2)^2}. \quad (4)$$

### 3.3 GRADIENT ANALYSIS FOR HYPERBOLIC NETWORK++ MLR

The derivative (Appendix A.2) of the HNN++ MLR formulation (Shimizu et al., 2021) with respect to its input  $\mathbf{x}_H$  is:

$$\begin{aligned} \frac{\partial}{\partial \mathbf{x}_H} v_{\mathbf{z},r}^{\text{HNN++}}(\mathbf{x}_H) &= \frac{2\|\mathbf{z}\|}{\sqrt{c}} \frac{1}{\sqrt{1 + F(\mathbf{x}_H)^2}} \frac{\partial}{\partial \mathbf{x}_H} F(\mathbf{x}_H), \quad \text{where} \\ \frac{\partial}{\partial \mathbf{x}_H} F(\mathbf{x}_H) &= \frac{2\sqrt{c} \cosh(2\sqrt{c}r)}{1 - c\|\mathbf{x}_H\|^2} \hat{\mathbf{z}} + \frac{4c \mathbf{x}_H \left( -\sinh(2\sqrt{c}r) + \sqrt{c} \cosh(2\sqrt{c}r) \langle \hat{\mathbf{z}}, \mathbf{x}_H \rangle \right)}{(1 - c\|\mathbf{x}_H\|^2)^2}. \end{aligned} \quad (5)$$

where  $\hat{\mathbf{z}} = \mathbf{z}/\|\mathbf{z}\|$  is the (normalized) Euclidean weight vector of the layer and  $r$  is a scalar bias term. The problematic term is the denominator  $(1 - c\|\mathbf{x}_H\|^2)^2$  in  $\partial F(\mathbf{x}_H)/\partial \mathbf{x}_H$ . It arises from the gradient of the conformal factor (Eq. 4), which causes gradient explosion near the Poincaré Ball boundary as  $\|\mathbf{x}_H\| \rightarrow 1/\sqrt{c}$ . Clipping  $\lambda_{\mathbf{x}_H}^c$  is undesirable because HNN++ MLR logits depend on  $\lambda_{\mathbf{x}_H}^c$  and alter the hyperbolic geometry by shifting decision boundaries, leading to performance plateaus. Hence, while HNN++ removes over-parameterization (Shimizu et al., 2021), it does not, by itself, resolve PPO training instabilities.

Next, we analyze the Jacobian of the Poincaré Ball exponential map  $\frac{\partial \mathbf{x}_H}{\partial \mathbf{x}_E}$  similar to Guo et al. (2022) (Appendix A.1):

$$\frac{\partial \mathbf{x}_H}{\partial \mathbf{x}_E} = \frac{\partial}{\partial \mathbf{x}_E} \exp_0(\mathbf{x}_E) = \frac{\tanh(\sqrt{c}\|\mathbf{x}_E\|)}{\sqrt{c}\|\mathbf{x}_E\|} \mathbf{I} + \left( \frac{\operatorname{sech}^2(\sqrt{c}\|\mathbf{x}_E\|)}{\|\mathbf{x}_E\|} - \frac{\tanh(\sqrt{c}\|\mathbf{x}_E\|)}{\sqrt{c}\|\mathbf{x}_E\|^2} \right) \frac{\mathbf{x}_E \mathbf{x}_E^\top}{\|\mathbf{x}_E\|}.$$

Although the exponential map Jacobian decays like  $O(\|\mathbf{x}_E\|^{-1})$ , the directional term (second summand) is highly sensitive to growing  $\|\mathbf{x}_E\|$ . Figures 2g and 2h show how volatile layer-wise gradients can get during training without proper handling. Cetin et al. (2023)'s S-RYM scaling factor  $\mathbf{x}_E \mapsto \mathbf{x}_E/\sqrt{d}$  keeps  $\|\mathbf{x}_E\|$  moderate, preventing  $\partial \exp_0(\mathbf{x}_E)/\partial \mathbf{x}_E$  from destabilizing the learning signal fed back to the encoder (Eq. 3) while reducing directional variability. Hence, regularizing Euclidean embeddings before the hyperbolic layers is a necessity for stable hyperbolic PPO agents.

### 3.4 GRADIENT ANALYSIS FOR HYPERBOLOID MLR

Prior work establishes that the Hyperboloid trains more stably than the Poincaré Ball (Mettes et al., 2024; Mishne et al., 2023; Bdeir et al., 2024) for two reasons. First, the Hyperboloid MLR score (Eq. 26) contains no conformal factor as it is not conformal to Euclidean space. Second, it neither multiplies nor divides by the Euclidean feature norm. As a result, its gradients avoid the instabilities of the Poincaré Ball. However, we will show in the following that the Jacobian  $\frac{\partial \mathbf{x}_H}{\partial \mathbf{v}} = \frac{\partial}{\partial \mathbf{v}} \exp_{\bar{0}}^c(\mathbf{v})$  of the Hyperboloid's exponential may still destabilize training. We denote  $\mathbf{v} = [0, \mathbf{x}_E] \in \mathcal{T}_{\bar{0}}\mathcal{M}$  as the Euclidean embeddings mapped into the tangent space of the Hyperboloid (cf. Section 2):

$$\frac{\partial \mathbf{x}_H}{\partial \mathbf{v}} = \begin{bmatrix} 0 & \sinh(\sqrt{c}\|\mathbf{x}_E\|) \frac{\mathbf{x}_E^\top}{\|\mathbf{x}_E\|} \\ \mathbf{0} & \frac{\sinh(\sqrt{c}\|\mathbf{x}_E\|)}{\sqrt{c}\|\mathbf{x}_E\|} \mathbf{I}_d + \frac{\sqrt{c}\|\mathbf{x}_E\| \cosh(\sqrt{c}\|\mathbf{x}_E\|) - \sinh(\sqrt{c}\|\mathbf{x}_E\|)}{\sqrt{c}\|\mathbf{x}_E\|^3} \mathbf{x}_E \mathbf{x}_E^\top \end{bmatrix}. \quad (6)$$

---

Equation 6 is a  $(1+s) \times (1+d)$  matrix, where the first column is zero. For large  $\|\mathbf{x}_E\|$ ,  $\sinh(\sqrt{c}\|\mathbf{x}_E\|)$  and  $\cosh(\sqrt{c}\|\mathbf{x}_E\|)$  grow exponentially, i.e., a faster rate than  $\sqrt{c}\|\mathbf{x}_E\|$ . Thus, the Hyperboloid exponential map can destabilize gradients when Euclidean feature norms grow, requiring regularization of  $\|\mathbf{x}_E\|$ .

Summarizing the findings in this section, we arrive at a more nuanced understanding of the training issues of hyperbolic deep RL agents: Policy breakdown and large-norm gradients in the encoder are a function of the hyperbolic layers used in the actor and the critic. The conformal factor, in particular, is a source of numerical instability in Riemannian optimization methods (Guo et al., 2022; Mishne et al., 2023). This numerical instability gets exacerbated by noisy gradients in actor-critic training, particularly from the critic’s side (Sutton & Barto, 2018; Nauman et al., 2024a). In the next section, we will show how our method HYPER++ deals with these issues.

## 4 STABILIZING HYPERBOLIC DEEP RL

In this part, we establish the components of our agent HYPER++: Section 4.1 proposes RMSNorm (Zhang & Sennrich, 2019) as an alternative to SpectralNorm. Section 4.2 introduces a novel feature scaling layer. Section 4.3 discusses how these components relate to the Hyperboloid. Beyond these design choices, we use a categorical loss to stabilize critic gradients (Imani & White, 2018; Farebrother et al., 2024) and to resolve an architectural mismatch in hyperbolic value learning. While Euclidean linear layers naturally support MSE regression over continuous values, hyperbolic MLR layers output classification-oriented hyperplane distances, making the categorical loss over discrete bins a better geometrical fit. Collectively, our components target complementary sources of instability in Equation 3: the categorical loss stabilizes the loss derivative (first term), Hyperboloid MLR stabilizes the hyperbolic layer Jacobian (second term), and RMSNorm with feature scaling stabilizes the Jacobian of the exponential map (third term). Figure 11 illustrates the underlying hybrid network architecture (Guo et al., 2022; Cetin et al., 2023) analyzed in the following.

### 4.1 REGULARIZATION

Here, we study how SpectralNorm (Miyato et al., 2018) affects the Euclidean embeddings produced by the encoder (cf. Figure 11). To this end, consider Lemma 4.1 which provides a bound on the norm of the embeddings computed by a single layer, depending on the input norm:

**Lemma 4.1.** *Let  $\mathbf{x} \in \mathbb{R}^n$ ,  $\mathbf{W} \in \mathbb{R}^{d \times n}$  and  $\mathbf{b} \in \mathbb{R}^d$ . Then, for any function  $f : \mathbb{R}^d \rightarrow \mathbb{R}^d$  with Lipschitz constant  $L$ , it holds that*

$$\|f(\mathbf{W}\mathbf{x} + \mathbf{b})\|_2 \leq \|f(\mathbf{0})\|_2 + L\|\mathbf{W}\|_2\|\mathbf{x}\|_2 + L\|\mathbf{b}\|_2. \quad (7)$$

*In particular, for ReLU activation functions and any normalized weight matrix  $\hat{\mathbf{W}}$ , we have*

$$\left\| \text{ReLU}(\hat{\mathbf{W}}\mathbf{x} + \mathbf{b}) \right\|_2 \leq \|\mathbf{x}\|_2 + \|\mathbf{b}\|_2. \quad (8)$$

Lemma 4.1 shows that for multi-layer encoders such as the one used by Cetin et al. (2023), applying SpectralNorm only to the last (linear) layer of the encoder is not sufficient to prevent the Euclidean embedding norms from growing via the preceding layers. To tangibly affect these norms, SpectralNorm must be applied to *every* layer of the encoder (Cetin et al., 2023). This constrains the Lipschitz constant of all layers and reduces expressivity by globally enforcing smoothness (Rosca et al., 2020; Cetin et al., 2023). Additionally, SpectralNorm incurs computational overhead from the power-iteration steps needed at each forward pass.

Ideally, we want to use regularization via spectral normalization only where needed and such that we can guarantee stable training, without limiting the expressivity of the entire Euclidean encoder. Proposition 4.2 shows that applying RMSNorm (Zhang & Sennrich, 2019) before the activation of the encoder’s last linear layer achieves stability without overly restricting its representational capacity (if the other layers are not regularized, their expressivity is not limited).

**Proposition 4.2.** *Let  $\mathbf{x} \in \mathbb{R}^d$  and  $f : \mathbb{R}^d \rightarrow \mathbb{R}^d$  with Lipschitz constant  $L$ . Then, for  $\hat{\mathbf{x}} = \frac{1}{\sqrt{d}}f(\text{RMS}(\mathbf{x}))$ , it holds that:*

$$\|\hat{\mathbf{x}}\|_2 < \frac{1}{\sqrt{d}}\|f(\mathbf{0})\|_2 + L, \quad \lambda_{\exp_{\bar{0}}(\hat{\mathbf{x}})} < 2 \cosh^2 \left( \sqrt{c} \left( \frac{1}{\sqrt{d}}\|f(\mathbf{0})\|_2 + L \right) \right). \quad (9)$$

Proposition 4.2 ensures stable hyperbolic operations for a broad class of activation functions. For common 1-Lipschitz activations such as TanH and ReLU, the bounds reduce to  $\|\hat{\mathbf{x}}\|_2 < 1$  and  $\|\exp_0(\hat{\mathbf{x}})\| < \frac{1}{\sqrt{c}} \tanh(\sqrt{c})$ . Unlike SpectralNorm, which constrains every encoder layer, we only require applying RMSNorm to the pre-activation output embeddings of the final linear layer. This retains the expressivity of each encoder layer. We use RMSNorm (Zhang & Sennrich, 2019) rather than LayerNorm (Ba et al., 2016) because we do not want the mean-centering in LayerNorm to distort the hierarchical structure of the hyperbolic embeddings. Additionally, RMSNorm brings three further advantages: it smoothes gradients, prevents dead ReLU or saturated TanH units (Zhang & Sennrich, 2019; Xu et al., 2019; Lyle et al., 2024), and supports arbitrary embedding dimensions  $d$ , since the bound in Proposition 4.2 is dimension-independent for activation functions with fixed point 0.

#### 4.2 LEARNED EUCLIDEAN FEATURE SCALING

Proposition 4.2 guarantees stability by bounding both Euclidean embedding norms and the conformal factor. However, this may still affect representational capacity in the hyperbolic layers of the agent. For example, with ReLU as the last encoder layer’s activation function and curvature  $c = 1$ , the bound restricts the Poincaré Ball radius to  $\|\mathbf{x}_H\|_2 \leq 0.76$  (see the proof of Proposition 4.2). Since the volume of a  $d$ -ball scales as  $V_d(r) = \frac{\pi^{d/2}}{\Gamma(\frac{d}{2}+1)} r^d \propto r^d$ , even a modest restriction of the radius causes an exponential loss of available volume in  $d$ . To mitigate this, we rescale the Euclidean tangent embeddings obtained after application of Proposition 4.2  $\hat{\mathbf{x}}_E$  by a learnable scalar  $\xi_\theta$ :

$$\hat{\mathbf{x}}_E^{\text{rescale}} = \rho_{\max} \sigma(\xi_\theta) \hat{\mathbf{x}}_E, \quad \rho_{\max} = \frac{\text{atanh}(\alpha)}{\sqrt{c}}, \quad (10)$$

where  $\sigma$  denotes the sigmoid function. By choosing this particular form for  $\rho_{\max}$ , we have that  $\|\exp_0(\hat{\mathbf{x}}_E^{\text{rescale}})\|_2 \leq \alpha/\sqrt{c}$  since  $\tanh(\sqrt{c} \rho_{\max}) = \alpha$ . Setting  $\alpha = 0.95$  (and  $c = 1$ ) expands the usable ball radius from 0.76 to 0.95, i.e., a volume gain of  $(0.95/0.76)^d$ . For  $d = 32$ , this is approximately  $1.2 \times 10^3$  more volume while still preventing the explosion of the conformal factor according to Proposition 4.2. Figure 3 illustrates the effect in 2D.

#### 4.3 HYPERBOLOID MODEL

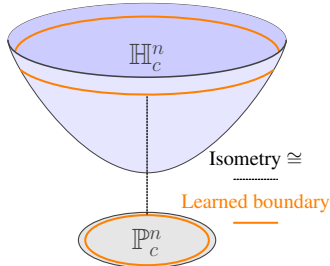


Figure 4: **Isometry between Poincaré Ball and Hyperboloid.**

Section 3.4 shows that the Hyperboloid avoids conformal factor instabilities and is therefore more robust against large norms. Yet, operations can become ill-conditioned far from the origin, i.e., when the sheet approaches the asymptotic null cone, and the Jacobian of the exponential map in Equation 6 gets more sensitive to large Euclidean norms. Since the Poincaré Ball and the Hyperboloid are isometric (Fig. 4) models, our stabilization strategy transfers: instead of capping the Poincaré Ball radius, we propose to apply RMSNorm and feature scaling before the last Euclidean activation to bound the Hyperboloid through its time component  $x_0$ . Corollary 4.3 formalizes this insight by combining Proposition 4.2 with the Poincaré Ball-Hyperboloid isometry (Chami et al., 2021; Mishne et al., 2023).

**Corollary 4.3.** *Let  $\hat{\mathbf{x}}_E \in \mathbb{R}^n$  be a point regularized by RMSNorm with learnable scaling, and  $\mathbf{x}_H = \exp_0(\hat{\mathbf{x}}_E) \in \mathbb{P}^n$ . Then, the maximum value of the time component  $x_0$  of that point on the Hyperboloid is*

$$x_0^{\max} = \frac{1 + c\|\mathbf{x}_H\|^2}{\sqrt{c}(1 - c\|\mathbf{x}_H\|^2)} = \frac{1 + \tanh^2(\sqrt{c}\|\hat{\mathbf{x}}_E\|)}{\sqrt{c}(1 - \tanh^2(\sqrt{c}\|\hat{\mathbf{x}}_E\|))}.$$

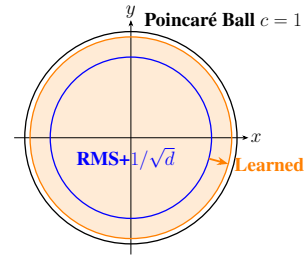


Figure 3: **Learned scaling effect.**

Figure 3 illustrates the learned scaling effect. The diagram shows a 2D plot of the Poincaré Ball  $c = 1$ . It features a blue circle representing the ball and an orange circle representing the rescaled ball. The radius of the blue circle is labeled 'RMS+1/sqrt(d)'. An arrow labeled 'Learned' points from the center of the blue circle to the center of the orange circle.

Section 3.4 shows that the Hyperboloid avoids conformal factor instabilities and is therefore more robust against large norms. Yet, operations can become ill-conditioned far from the origin, i.e., when the sheet approaches the asymptotic null cone, and the Jacobian of the exponential map in Equation 6 gets more sensitive to large Euclidean norms. Since the Poincaré Ball and the Hyperboloid are isometric (Fig. 4) models, our stabilization strategy transfers: instead of capping the Poincaré Ball radius, we propose to apply RMSNorm and feature scaling before the last Euclidean activation to bound the Hyperboloid through its time component  $x_0$ . Corollary 4.3 formalizes this insight by combining Proposition 4.2 with the Poincaré Ball-Hyperboloid isometry (Chami et al., 2021; Mishne et al., 2023).

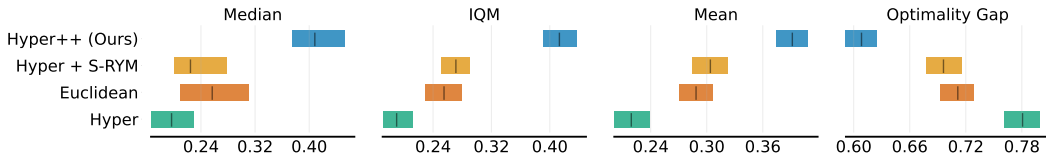
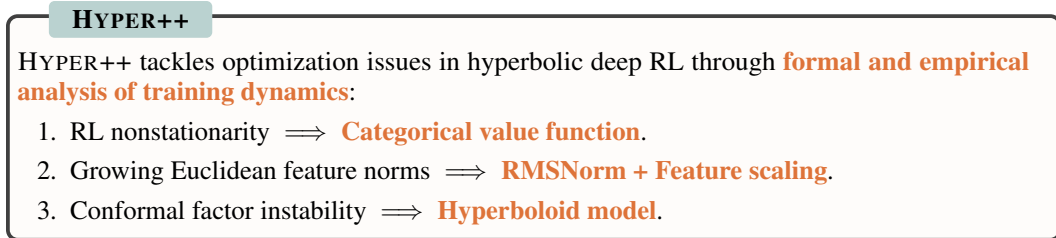


Figure 5: **Normalized test rewards on ProcGen.** HYPER++ outperforms baselines for all aggregation methods without increasing variance (as measured by the bootstrap confidence interval). We report median, interquartile mean (IQM), mean, and optimality gap, which is  $1 - \text{IQM}$ .

Since the time and space components are dependent (cf. Section 2.2), bounding the maximum norm of  $x_0^{\max}$  also ensures that the space component  $x_s$  remains bounded. Therefore, we also apply regularization with RMSNorm and learned scaling when training agents using the Hyperboloid. In Section 5.2, we show that this approach works well empirically. Our proposed agent HYPER++ is visualized in Figure 11 (Appendix) consists of the following components:



## 5 EXPERIMENTS

We evaluate HYPER++ on ProcGen (Cobbe et al., 2020) with PPO (Schulman et al., 2017) in Section 5.1 and provide ablation studies in Section 5.2. We test performance with the off-policy algorithm DDQN (van Hasselt et al., 2016) on a subset of Atari games (Bellemare et al., 2015; Towers et al., 2024; Aitchison et al., 2023). Unless stated otherwise, error bands show one standard deviation. Wall-clock times are reported in Appendix D.1.

### 5.1 PROCGEN

Figure 5 shows aggregate test rewards using normalized test rewards for 25M time steps on ProcGen. We normalize using random performance as the minimum and either a theoretical or empirically determined maximum (Cobbe et al., 2020). We use the reliable library (Agarwal et al., 2021) to compute aggregate metrics such as the interquartile-mean (IQM) and the optimality gap with bootstrap confidence intervals.

HYPER++ outperforms Poincaré agents with and without S-RYM, as well as the Euclidean baseline. The per-game curves in Figure 6 match our findings: hyperbolic agents beat Euclidean ones on BIGFISH and DODGEBALL, while performance on STARPILOT and FRUITBOT saturates near the ceiling for all methods. Tables 6 and 7 show HYPER++ winning head-to-head vs. Hyper+S-RYM in 8/16 games on the train set and 11/16 games on the test set.

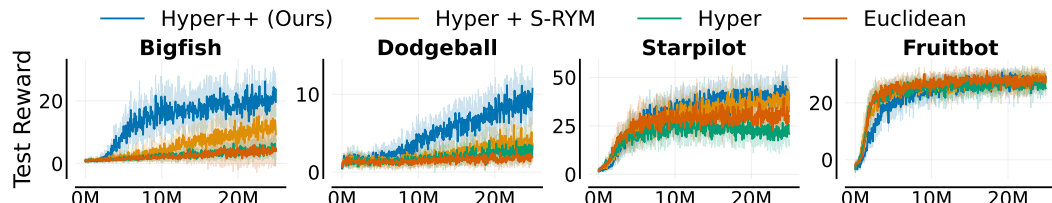
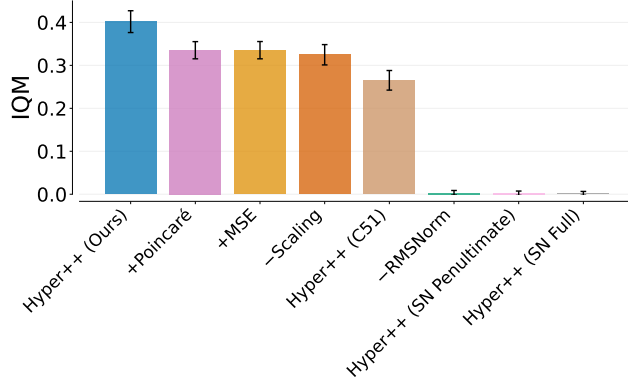


Figure 6: **Learning curves for PPO on ProcGen.** We report the mean test rewards over six seeds on the same environments as Cetin et al. (2023).

## 5.2 ABLATION STUDIES

Figure 7 presents ablations of HYPER++’s components using test IQM with bootstrapped confidence intervals. We begin with the most critical component: normalization. Removing RMSNorm (Zhang & Sennrich, 2019) and  $1/\sqrt{d}$  feature scaling causes complete learning failure (-RMSNorm), confirming the predictions of Proposition 4.2.



**Figure 7: Ablation studies on ProcGen with Hyperbolic geometry.** We report the test interquartile mean (IQM) across six seeds with bootstrap confidence intervals. – indicates that a component is removed from HYPER++, + indicates a component replacing its analog.

2017) distributional loss for HL-Gauss performs even worse than the Poincaré ball instead of the hyperboloid model (+Poincaré) leads to a modest drop in performance, which is expected given their isometry (Corollary 4.3).

We further validate Lemma 4.1 by testing SpectralNorm (Miyato et al., 2018) as an alternative to RMSNorm in two configurations: applying SpectralNorm to the complete Euclidean encoder (HYPER++ (SN Full)) and applying it only to the penultimate layer (HYPER++ (SN Penultimate)). In both cases, the agent fails to learn entirely. This underscores the critical importance of RMSNorm for obtaining the bounded feature norms guaranteed by Proposition 4.2.

Finally, Figure 8 isolates the contribution of hyperbolic representations by evaluating Euclidean agents equipped with HL-Gauss, RMSNorm, and our full regularization combination. For Euclidean representations, the HL-Gauss loss (Euclidean+Categorical) performs worse than MSE. Adding RMSNorm to Euclidean agents improves performance, and equipping Euclidean agents with our full method yields an IQM of 0.35, which is slightly better than HYPER++ with the Poincaré ball (IQM=0.34). However, HYPER++ with the Hyperboloid achieves the best overall performance (IQM=0.40). The underperformance of Euclidean+HL-Gauss relative to Euclidean+MSE indicates that categorical losses are particularly well-suited for hyperbolic agents, due to being a better geometric fit for the signed distances produced by the critic’s hyperbolic MLR layer. Overall, our results demonstrate that hyperbolic representations can benefit deep RL agents, but require an optimization-friendly approach to hyperbolic geometry to realize these benefits. We present complete ablation results in Tables 9 and 10. In summary, every ablation underperforms HYPER++ with the Hyperboloid, confirming the synergistic interactions between hyperbolic geometry and our method’s components.

This failure manifests as large embedding norms and near-zero gradients in the encoder’s final layer (Figure 14), providing empirical support for the theoretical analysis in Section 3 and Proposition 4.2. The next most important architectural choice is learned scaling (-Scaling), which we attribute to its synergy with RMSNorm. Among the loss function variants, replacing the categorical HL-Gauss loss (Imani & White, 2018) with MSE (+MSE) degrades performance, though not uniformly across all games. This aligns with the findings of Farebrother et al. (2024), who similarly observe that HL-Gauss does not consistently improve performance on all environments. Interestingly, substituting the C51 (Bellemare et al.,

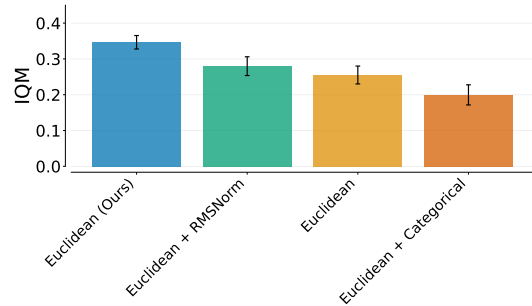


**Figure 8: Ablation studies on ProcGen with Euclidean geometry.** We report the test interquartile mean (IQM) across six seeds with bootstrap confidence intervals.

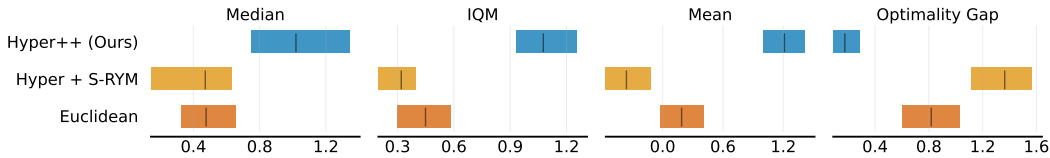


Figure 9: **Human-normalized performance for DDQN on Atari-5.** All agents are trained for 10M steps and five seeds. HYPER++ strongly improves over the baselines.

### 5.3 ATARI DDQN

We evaluate our algorithm using the value-based off-policy algorithm DDQN (van Hasselt et al., 2016) (Appendix B.2). We focus on the Atari-5 subset of games (Aitchison et al., 2023), which consists of NAMETHISGAME, PHOENIX, BATTLEZONE, DOUBLE DUNK, and Q\*BERT. This subset has been shown to be the most predictive of overall performance across all Atari environments (Bellemare et al., 2015; Towers et al., 2024). We train each agent for 10M steps and five random seeds. Figure 9 shows the final episode rewards achieved by each method. HYPER++ substantially outperforms the baselines across all five games in all metrics. Appendix E.5 provides the full learning curves for each individual game. We find that performance varies across games: our method achieves its strongest gains on NAMETHISGAME and Q\*BERT. On PHOENIX, HYPER++ exhibits strong initial performance but subsequently plateaus, mirroring the behavior of the baseline agents. This plateauing is consistent with plasticity loss being a confounding factor on this particular game (Klein et al., 2024). To further assess the generality of our modifications, we conduct an ablation study on NAMETHISGAME using Polyak updates for the target network instead of the standard hard replacement updates. We perform this ablation on NAMETHISGAME, as it is the single most representative game in the Atari benchmark according to Aitchison et al. (2023). As shown in Figure E.6, Polyak updates introduce only minor differences in performance, suggesting that our method is robust to this design choice.

## 6 RELATED WORK

**Hyperbolic deep learning** has progressed quickly from early hyperbolic neural networks and Riemannian optimization (Ganea et al., 2018; Bécigneul & Ganea, 2019), which Cetin et al. (2023) adapt to RL. Parameter redundancy in Poincaré Ball MLR was reduced by Shimizu et al. (2021). Fully hyperbolic architectures on the Hyperboloid now include transformers and convolutional networks, as well as a Hyperboloid MLR layer (Chen et al., 2022; Bdeir et al., 2024). Mettes et al. (2024) survey this literature from a vision perspective. Optimization and numerical stability have been analyzed independently (Mishne et al., 2023; Guo et al., 2022). We study optimization problems of hyperbolic networks within RL and propose a principled solution.

**Reinforcement learning.** We focus on PPO (Schulman et al., 2017), which remains under active study (Andrychowicz et al., 2021; Moalla et al., 2024) because of its strong performance. Several works show that regularization can improve deep RL training; with LayerNorm being widely adopted in the deep RL (Henderson et al., 2018; Ba et al., 2016; Lyle et al., 2023; Nauman et al., 2024b; Lee et al., 2025; Gallici et al., 2025). Instead, we regularize our agent using RMSNorm (Zhang & Sennrich, 2019), preventing interference with hyperbolic representations. A separate line of research is stabilizing value function learning via categorical objectives (Bellemare et al., 2017; Schriftwieser et al., 2020; Imani & White, 2018; Farebrother et al., 2024), which we extend to hyperbolic PPO.

## 7 LIMITATIONS AND CONCLUSION

**Limitations and Future Work.** Our analysis takes an optimization-centric view, focusing on training dynamics and the question of *how* hyperbolic deep RL learns, rather than *what* structures their representations capture. We also do not address which environments are most suited to hyperbolic representations. Moreover, the interaction between geometric choices and the design of different deep RL algorithms, remains unexplored. Each of these directions is an exciting avenue for future work.

**Conclusion.** Our work analyzes gradients in the Poincaré Ball and Hyperboloid, linking large-norm embeddings to PPO trust-region breakdowns. Based on these insights, we introduce HYPER++, which combines RMSNorm with learned feature scaling and a categorical value loss to stabilize hyperbolic

---

deep RL. On ProcGen, HYPER++ improves performance and substantially reduces wall-clock time compared to existing hyperbolic PPO agents. Our findings transfer to Atari and DDQN with strong gains, indicating broader applicability beyond PPO.

#### REPRODUCIBILITY

We will make our code publicly available on GitHub. Appendix A contains the derivations for our gradient analysis and proofs for our theoretical results. In Appendix D, we state agent architecture, hyperparameters, relevant implementation details, and hardware used. In Appendix C.3 we discuss differences in results to existing works.

#### USAGE OF LARGE LANGUAGE MODELS (LLMs)

During this project, we used LLMs as an assistive tool. In the early stages of our project, we used LLMs for literature search and paper summarization. During the implementation phase, we used code assistants to support repetitive coding tasks such as Matplotlib figure generation. For the paper, LLMs were used as a tool to iterate on our writing. An example use case is paragraph shortening with “Shorten this paragraph.” All LLM outputs used in this paper were thoroughly reviewed to ensure accuracy. LLMs were not used for idea generation, experimental design, or for proofs. Mathematical expressions were derived independently.

#### ETHICS STATEMENT

Our work advances the fundamental capabilities of hyperbolic deep RL agents and has no direct ethical implications by itself. We cannot rule out that unethical uses could occur in downstream applications because RL and PPO, in particular, are used to train LLMs, and hyperbolic embeddings are well-suited for text data. However, such uses would require significant extensions and modifications beyond the work submitted here.

#### AUTHOR CONTRIBUTIONS

If you’d like to, you may include a section for author contributions as is done in many journals. This is optional and at the discretion of the authors.

#### ACKNOWLEDGMENTS

This work has been funded in parts by the Vienna Science and Technology Fund (WWTF) [10.47379/ICT20058]. We acknowledge EuroHPC JU for awarding the project ID EHPC-DEV-2025D08-024 access to the Luxembourg national supercomputer, MeluXina, and the Spanish supercomputer, MareNostrum. The authors gratefully acknowledge the LuxProvide and Barcelona Supercomputing Center for their expert support. Without Nikolaus Süß’ tireless work maintaining our research group’s computing infrastructure, this work would not have been possible. We are deeply grateful.

#### REFERENCES

Rishabh Agarwal, Max Schwarzer, Pablo Samuel Castro, Aaron C. Courville, and Marc G. Bellemare. Deep reinforcement learning at the edge of the statistical precipice. In Marc’Aurelio Ranzato, Alina Beygelzimer, Yann N. Dauphin, Percy Liang, and Jennifer Wortman Vaughan (eds.), *Advances in Neural Information Processing Systems 34: Annual Conference on Neural Information Processing Systems 2021, NeurIPS 2021, December 6-14, 2021, virtual*, pp. 29304–29320, 2021. URL <https://proceedings.neurips.cc/paper/2021/hash/f514cec81cb148559cf475e7426eed5e-Abstract.html>.

Matthew Aitchison, Penny Sweetser, and Marcus Hutter. Atari-5: Distilling the arcade learning environment down to five games. In Andreas Krause, Emma Brunskill, Kyunghyun Cho, Barbara Engelhardt, Sivan Sabato, and Jonathan Scarlett (eds.), *International Conference on Machine Learning, ICML 2023, 23-29 July 2023, Honolulu, Hawaii, USA*, volume 202 of *Proceedings of Machine Learning Research*, pp. 421–438. PMLR, 2023. URL <https://proceedings.mlr.press/v202/aitchison23a.html>.

---

Marcin Andrychowicz, Anton Raichuk, Piotr Stanczyk, Manu Orsini, Sertan Girgin, Raphaël Marinier, Léonard Hussenot, Matthieu Geist, Olivier Pietquin, Marcin Michalski, Sylvain Gelly, and Olivier Bachem. What matters for on-policy deep actor-critic methods? A large-scale study. In *9th International Conference on Learning Representations, ICLR 2021, Virtual Event, Austria, May 3-7, 2021*. OpenReview.net, 2021. URL <https://openreview.net/forum?id=nIAxjsniDzg>.

Lei Jimmy Ba, Jamie Ryan Kiros, and Geoffrey E. Hinton. Layer normalization. *CoRR*, abs/1607.06450, 2016. URL <http://arxiv.org/abs/1607.06450>.

Ahmad Bdeir, Kristian Schwethelm, and Niels Landwehr. Fully hyperbolic convolutional neural networks for computer vision. In *The Twelfth International Conference on Learning Representations, ICLR 2024, Vienna, Austria, May 7-11, 2024*. OpenReview.net, 2024. URL <https://openreview.net/forum?id=ekz1hN5QNh>.

Gary Bécigneul and Octavian-Eugen Ganea. Riemannian adaptive optimization methods. In *7th International Conference on Learning Representations, ICLR 2019, New Orleans, LA, USA, May 6-9, 2019*. OpenReview.net, 2019. URL <https://openreview.net/forum?id=r1eiqi09K7>.

Marc G. Bellemare, Yavar Naddaf, Joel Veness, and Michael Bowling. The arcade learning environment: An evaluation platform for general agents (extended abstract). In Qiang Yang and Michael J. Wooldridge (eds.), *Proceedings of the Twenty-Fourth International Joint Conference on Artificial Intelligence, IJCAI 2015, Buenos Aires, Argentina, July 25-31, 2015*, pp. 4148–4152. AAAI Press, 2015. URL <http://ijcai.org/Abstract/15/585>.

Marc G. Bellemare, Will Dabney, and Rémi Munos. A distributional perspective on reinforcement learning. In Doina Precup and Yee Whye Teh (eds.), *Proceedings of the 34th International Conference on Machine Learning, ICML 2017, Sydney, NSW, Australia, 6-11 August 2017*, volume 70 of *Proceedings of Machine Learning Research*, pp. 449–458. PMLR, 2017. URL <http://proceedings.mlr.press/v70/bellemare17a.html>.

János Bolyai. *The Science Absolute of Space...*, volume 3. The Neomon, 1896.

Edoardo Cetin, Benjamin Paul Chamberlain, Michael M. Bronstein, and Jonathan J. Hunt. Hyperbolic deep reinforcement learning. In *The Eleventh International Conference on Learning Representations, ICLR 2023, Kigali, Rwanda, May 1-5, 2023*. OpenReview.net, 2023. URL <https://openreview.net/forum?id=TfBHFLgv77>.

Ines Chami, Zhitao Ying, Christopher Ré, and Jure Leskovec. Hyperbolic graph convolutional neural networks. In Hanna M. Wallach, Hugo Larochelle, Alina Beygelzimer, Florence d’Alché-Buc, Emily B. Fox, and Roman Garnett (eds.), *Advances in Neural Information Processing Systems 32: Annual Conference on Neural Information Processing Systems 2019, NeurIPS 2019, December 8-14, 2019, Vancouver, BC, Canada*, pp. 4869–4880, 2019. URL <https://proceedings.neurips.cc/paper/2019/hash/0415740eaa4d9dec8da001d3fd805f-Abstract.html>.

Ines Chami, Albert Gu, Dat P Nguyen, and Christopher Ré. Horopca: Hyperbolic dimensionality reduction via horospherical projections. In *International Conference on Machine Learning*, pp. 1419–1429. PMLR, 2021.

Weize Chen, Xu Han, Yankai Lin, Hexu Zhao, Zhiyuan Liu, Peng Li, Maosong Sun, and Jie Zhou. Fully hyperbolic neural networks. In Smaranda Muresan, Preslav Nakov, and Aline Villavicencio (eds.), *Proceedings of the 60th Annual Meeting of the Association for Computational Linguistics (Volume 1: Long Papers), ACL 2022, Dublin, Ireland, May 22-27, 2022*, pp. 5672–5686. Association for Computational Linguistics, 2022. doi: 10.18653/V1/2022.AC-LONG.389. URL <https://doi.org/10.18653/v1/2022.acl-long.389>.

Karl Cobbe, Christopher Hesse, Jacob Hilton, and John Schulman. Leveraging procedural generation to benchmark reinforcement learning. In *Proceedings of the 37th International Conference on Machine Learning, ICML 2020, 13-18 July 2020, Virtual Event*, volume 119 of *Proceedings of Machine Learning Research*, pp. 2048–2056. PMLR, 2020. URL <http://proceedings.mlr.press/v119/cobbe20a.html>.

---

Aleksandr Ermolov, Leyla Mirvakhabova, Valentin Khrulkov, Nicu Sebe, and Ivan V. Oseledets. Hyperbolic vision transformers: Combining improvements in metric learning. In *IEEE/CVF Conference on Computer Vision and Pattern Recognition, CVPR 2022, New Orleans, LA, USA, June 18-24, 2022*, pp. 7399–7409. IEEE, 2022. doi: 10.1109/CVPR52688.2022.00726. URL <https://doi.org/10.1109/CVPR52688.2022.00726>.

Lasse Espeholt, Hubert Soyer, Rémi Munos, Karen Simonyan, Volodymyr Mnih, Tom Ward, Yotam Doron, Vlad Firoiu, Tim Harley, Iain Dunning, Shane Legg, and Koray Kavukcuoglu. IMPALA: scalable distributed deep-rl with importance weighted actor-learner architectures. In Jennifer G. Dy and Andreas Krause (eds.), *Proceedings of the 35th International Conference on Machine Learning, ICML 2018, Stockholmsmässan, Stockholm, Sweden, July 10-15, 2018*, volume 80 of *Proceedings of Machine Learning Research*, pp. 1406–1415. PMLR, 2018. URL <http://proceedings.mlr.press/v80/espeholt18a.html>.

Jesse Farebrother, Jordi Orbay, Quan Vuong, Adrien Ali Taïga, Yevgen Chebotar, Ted Xiao, Alex Irpan, Sergey Levine, Pablo Samuel Castro, Aleksandra Faust, Aviral Kumar, and Rishabh Agarwal. Stop regressing: Training value functions via classification for scalable deep RL. In *Forty-first International Conference on Machine Learning, ICML 2024, Vienna, Austria, July 21-27, 2024*. OpenReview.net, 2024. URL <https://openreview.net/forum?id=dVpFKfqF3R>.

Matteo Gallici, Mattie Fellows, Benjamin Ellis, Bartomeu Pou, Ivan Masmitja, Jakob Nicolaus Foerster, and Mario Martin. Simplifying deep temporal difference learning. In *The Thirteenth International Conference on Learning Representations, ICLR 2025, Singapore, April 24-28, 2025*. OpenReview.net, 2025. URL <https://openreview.net/forum?id=7IzeL0kflu>.

Octavian-Eugen Ganea, Gary Bécigneul, and Thomas Hofmann. Hyperbolic neural networks. In Samy Bengio, Hanna M. Wallach, Hugo Larochelle, Kristen Grauman, Nicolò Cesa-Bianchi, and Roman Garnett (eds.), *Advances in Neural Information Processing Systems 31: Annual Conference on Neural Information Processing Systems 2018, NeurIPS 2018, December 3-8, 2018, Montréal, Canada*, pp. 5350–5360, 2018. URL <https://proceedings.neurips.cc/paper/2018/hash/dbab2adc8f9d078009ee3fa810bea142-Abstract.html>.

M Gromov. Hyperbolic groups. *Essays in Group Theory*, pages Springer-Verlag, 1987.

Yunhui Guo, Xudong Wang, Yubei Chen, and Stella X. Yu. Clipped hyperbolic classifiers are super-hyperbolic classifiers. In *IEEE/CVF Conference on Computer Vision and Pattern Recognition, CVPR 2022, New Orleans, LA, USA, June 18-24, 2022*, pp. 1–10. IEEE, 2022. doi: 10.1109/CVPR52688.2022.00010. URL <https://doi.org/10.1109/CVPR52688.2022.00010>.

Peter Henderson, Riashat Islam, Philip Bachman, Joelle Pineau, Doina Precup, and David Meger. Deep reinforcement learning that matters. In Sheila A. McIlraith and Kilian Q. Weinberger (eds.), *Proceedings of the Thirty-Second AAAI Conference on Artificial Intelligence, (AAAI-18), the 30th innovative Applications of Artificial Intelligence (IAAI-18), and the 8th AAAI Symposium on Educational Advances in Artificial Intelligence (EAAI-18), New Orleans, Louisiana, USA, February 2-7, 2018*, pp. 3207–3214. AAAI Press, 2018. doi: 10.1609/AAAI.V32I1.11694. URL <https://doi.org/10.1609/aaai.v32i1.11694>.

Shengyi Huang, Rousslan Fernand Julien Dossa, Chang Ye, Jeff Braga, Dipam Chakraborty, Kinal Mehta, and João G. M. Araújo. Cleanrl: High-quality single-file implementations of deep reinforcement learning algorithms. *J. Mach. Learn. Res.*, 23:274:1–274:18, 2022. URL <https://jmlr.org/papers/v23/21-1342.html>.

Ehsan Imani and Martha White. Improving regression performance with distributional losses. In Jennifer G. Dy and Andreas Krause (eds.), *Proceedings of the 35th International Conference on Machine Learning, ICML 2018, Stockholmsmässan, Stockholm, Sweden, July 10-15, 2018*, volume 80 of *Proceedings of Machine Learning Research*, pp. 2162–2171. PMLR, 2018. URL <http://proceedings.mlr.press/v80/imani18a.html>.

Isay Katsman and Anna Gilbert. Shedding light on problems with hyperbolic graph learning. *Trans. Mach. Learn. Res.*, 2025, 2025. URL <https://openreview.net/forum?id=rKAkp1f3R7>.

---

Diederik P. Kingma and Jimmy Ba. Adam: A method for stochastic optimization. In Yoshua Bengio and Yann LeCun (eds.), *3rd International Conference on Learning Representations, ICLR 2015, San Diego, CA, USA, May 7-9, 2015, Conference Track Proceedings*, 2015. URL <http://arxiv.org/abs/1412.6980>.

Timo Klein, Lukas Miklautz, Kevin Sidak, Claudia Plant, and Sebastian Tschiatschek. Plasticity loss in deep reinforcement learning: A survey. *CoRR*, abs/2411.04832, 2024. doi: 10.48550/ARXIV.2411.04832. URL <https://doi.org/10.48550/arXiv.2411.04832>.

Guy Lebanon and John D. Lafferty. Hyperplane margin classifiers on the multinomial manifold. In Carla E. Brodley (ed.), *Machine Learning, Proceedings of the Twenty-first International Conference (ICML 2004), Banff, Alberta, Canada, July 4-8, 2004*, volume 69 of *ACM International Conference Proceeding Series*. ACM, 2004. doi: 10.1145/1015330.1015333. URL <https://doi.org/10.1145/1015330.1015333>.

Hojoon Lee, Dongyoong Hwang, Donghu Kim, Hyunseung Kim, Jun Jet Tai, Kaushik Subramanian, Peter R. Wurman, Jaegul Choo, Peter Stone, and Takuma Seno. Simba: Simplicity bias for scaling up parameters in deep reinforcement learning. In *The Thirteenth International Conference on Learning Representations, ICLR 2025, Singapore, April 24-28, 2025*. OpenReview.net, 2025. URL <https://openreview.net/forum?id=jXLiDKsuDo>.

Nikolai Ivanovich Lobachevskii. *Geometrical researches on the theory of parallels*. University of Texas, 1891.

Clare Lyle, Zeyu Zheng, Evgenii Nikishin, Bernardo Ávila Pires, Razvan Pascanu, and Will Dabney. Understanding plasticity in neural networks. In Andreas Krause, Emma Brunskill, Kyunghyun Cho, Barbara Engelhardt, Sivan Sabato, and Jonathan Scarlett (eds.), *International Conference on Machine Learning, ICML 2023, 23-29 July 2023, Honolulu, Hawaii, USA*, volume 202 of *Proceedings of Machine Learning Research*, pp. 23190–23211. PMLR, 2023. URL <https://proceedings.mlr.press/v202/lyle23b.html>.

Clare Lyle, Zeyu Zheng, Khimya Khetarpal, James Martens, Hado Philip van Hasselt, Razvan Pascanu, and Will Dabney. Normalization and effective learning rates in reinforcement learning. In Amir Globersons, Lester Mackey, Danielle Belgrave, Angela Fan, Ulrich Paquet, Jakub M. Tomczak, and Cheng Zhang (eds.), *Advances in Neural Information Processing Systems 38: Annual Conference on Neural Information Processing Systems 2024, NeurIPS 2024, Vancouver, BC, Canada, December 10 - 15, 2024*, 2024. URL [http://papers.nips.cc/paper\\_files/paper/2024/hash/c04d37be05ba74419d2d5705972a9d64-Abstract-Conference.html](http://papers.nips.cc/paper_files/paper/2024/hash/c04d37be05ba74419d2d5705972a9d64-Abstract-Conference.html).

Emile Mathieu, Charline Le Lan, Chris J. Maddison, Ryota Tomioka, and Yee Whye Teh. Continuous hierarchical representations with poincaré variational auto-encoders. In Hanna M. Wallach, Hugo Larochelle, Alina Beygelzimer, Florence d’Alché-Buc, Emily B. Fox, and Roman Garnett (eds.), *Advances in Neural Information Processing Systems 32: Annual Conference on Neural Information Processing Systems 2019, NeurIPS 2019, December 8-14, 2019, Vancouver, BC, Canada*, pp. 12544–12555, 2019. URL <https://proceedings.neurips.cc/paper/2019/hash/0ec04cb3912c4f08874dd03716f80df1-Abstract.html>.

Pascal Mettes, Mina Ghadimi Atigh, Martin Keller-Ressel, Jeffrey Gu, and Serena Yeung. Hyperbolic deep learning in computer vision: A survey. *Int. J. Comput. Vis.*, 132(9):3484–3508, 2024. doi: 10.1007/S11263-024-02043-5. URL <https://doi.org/10.1007/s11263-024-02043-5>.

Gal Mishne, Zhengchao Wan, Yusu Wang, and Sheng Yang. The numerical stability of hyperbolic representation learning. In Andreas Krause, Emma Brunskill, Kyunghyun Cho, Barbara Engelhardt, Sivan Sabato, and Jonathan Scarlett (eds.), *International Conference on Machine Learning, ICML 2023, 23-29 July 2023, Honolulu, Hawaii, USA*, volume 202 of *Proceedings of Machine Learning Research*, pp. 24925–24949. PMLR, 2023. URL <https://proceedings.mlr.press/v202/mishne23a.html>.

Takeru Miyato, Toshiki Kataoka, Masanori Koyama, and Yuichi Yoshida. Spectral normalization for generative adversarial networks. In *6th International Conference on Learning Representations, ICLR 2018, Vancouver, BC, Canada, April 30 - May 3, 2018, Conference Track Proceedings*. OpenReview.net, 2018. URL <https://openreview.net/forum?id=B1QRgziT->.

---

Volodymyr Mnih, Koray Kavukcuoglu, David Silver, Andrei A. Rusu, Joel Veness, Marc G. Bellemare, Alex Graves, Martin A. Riedmiller, Andreas Fidjeland, Georg Ostrovski, Stig Petersen, Charles Beattie, Amir Sadik, Ioannis Antonoglou, Helen King, Dharshan Kumaran, Daan Wierstra, Shane Legg, and Demis Hassabis. Human-level control through deep reinforcement learning. *Nat.*, 518(7540):529–533, 2015. doi: 10.1038/NATURE14236. URL <https://doi.org/10.1038/nature14236>.

Skander Moalla, Andrea Miele, Daniil Pyatko, Razvan Pascanu, and Caglar Gulcehre. No representation, no trust: Connecting representation, collapse, and trust issues in PPO. In Amir Globersons, Lester Mackey, Danielle Belgrave, Angela Fan, Ulrich Paquet, Jakub M. Tomczak, and Cheng Zhang (eds.), *Advances in Neural Information Processing Systems 38: Annual Conference on Neural Information Processing Systems 2024, NeurIPS 2024, Vancouver, BC, Canada, December 10 - 15, 2024*, 2024. URL [http://papers.nips.cc/paper\\_files/paper/2024/hash/81166fb9cc5adf14031cdb69d3fd6a8-Abstract-Conference.html](http://papers.nips.cc/paper_files/paper/2024/hash/81166fb9cc5adf14031cdb69d3fd6a8-Abstract-Conference.html).

Michał Nauman, Michał Bortkiewicz, Piotr Miłos, Tomasz Trzcinski, Mateusz Ostaszewski, and Marek Cygan. Overestimation, overfitting, and plasticity in actor-critic: the bitter lesson of reinforcement learning. In *Forty-first International Conference on Machine Learning, ICML 2024, Vienna, Austria, July 21-27, 2024*. OpenReview.net, 2024a. URL <https://openreview.net/forum?id=5vZzmCeTYu>.

Michał Nauman, Mateusz Ostaszewski, Krzysztof Jankowski, Piotr Miłos, and Marek Cygan. Bigger, regularized, optimistic: scaling for compute and sample efficient continuous control. In Amir Globersons, Lester Mackey, Danielle Belgrave, Angela Fan, Ulrich Paquet, Jakub M. Tomczak, and Cheng Zhang (eds.), *Advances in Neural Information Processing Systems 38: Annual Conference on Neural Information Processing Systems 2024, NeurIPS 2024, Vancouver, BC, Canada, December 10 - 15, 2024*, 2024b. URL [http://papers.nips.cc/paper\\_files/paper/2024/hash/cd3b5d2ed967e906af24b33d6a356cac-Abstract-Conference.html](http://papers.nips.cc/paper_files/paper/2024/hash/cd3b5d2ed967e906af24b33d6a356cac-Abstract-Conference.html).

Long Ouyang, Jeffrey Wu, Xu Jiang, Diogo Almeida, Carroll L. Wainwright, Pamela Mishkin, Chong Zhang, Sandhini Agarwal, Katarina Slama, Alex Ray, John Schulman, Jacob Hilton, Fraser Kelton, Luke Miller, Maddie Simens, Amanda Askell, Peter Welinder, Paul F. Christiano, Jan Leike, and Ryan Lowe. Training language models to follow instructions with human feedback. In Sanmi Koyejo, S. Mohamed, A. Agarwal, Danielle Belgrave, K. Cho, and A. Oh (eds.), *Advances in Neural Information Processing Systems 35: Annual Conference on Neural Information Processing Systems 2022, NeurIPS 2022, New Orleans, LA, USA, November 28 - December 9, 2022*, 2022. URL [http://papers.nips.cc/paper\\_files/paper/2022/hash/b1efde53be364a73914f58805a001731-Abstract-Conference.html](http://papers.nips.cc/paper_files/paper/2022/hash/b1efde53be364a73914f58805a001731-Abstract-Conference.html).

Avik Pal, Max van Spengler, Guido Maria D’Amely di Melendugno, Alessandro Flaborea, Fabio Galasso, and Pascal Mettes. Compositional entailment learning for hyperbolic vision-language models. In *The Thirteenth International Conference on Learning Representations, ICLR 2025, Singapore, April 24-28, 2025*. OpenReview.net, 2025. URL <https://openreview.net/forum?id=3i13Gev2hV>.

Mihaela Rosca, Theophane Weber, Arthur Gretton, and Shakir Mohamed. A case for new neural network smoothness constraints. In Jessica Zosa Forde, Francisco J. R. Ruiz, Melanie F. Pradier, and Aaron Schein (eds.), *“I Can’t Believe It’s Not Better!” at NeurIPS Workshops, Virtual, December 12, 2020*, volume 137 of *Proceedings of Machine Learning Research*, pp. 21–32. PMLR, 2020. URL <https://proceedings.mlr.press/v137/rosc20a.html>.

Omar Salemohamed, Edoardo Cetin, Sai Rajeswar, and Arnab Kumar Mondal. Hyperbolic deep reinforcement learning for continuous control. In Krystal Maughan, Rosanne Liu, and Thomas F. Burns (eds.), *The First Tiny Papers Track at ICLR 2023, Tiny Papers @ ICLR 2023, Kigali, Rwanda, May 5, 2023*. OpenReview.net, 2023. URL <https://openreview.net/forum?id=Mrz9PgP3st>.

Rik Sarkar. Low distortion delaunay embedding of trees in hyperbolic plane. In *International symposium on graph drawing*, pp. 355–366. Springer, 2011.

---

Julian Schrittwieser, Ioannis Antonoglou, Thomas Hubert, Karen Simonyan, Laurent Sifre, Simon Schmitt, Arthur Guez, Edward Lockhart, Demis Hassabis, Thore Graepel, Timothy P. Lillicrap, and David Silver. Mastering atari, go, chess and shogi by planning with a learned model. *Nat.*, 588(7839):604–609, 2020. doi: 10.1038/S41586-020-03051-4. URL <https://doi.org/10.1038/s41586-020-03051-4>.

John Schulman, Sergey Levine, Pieter Abbeel, Michael I. Jordan, and Philipp Moritz. Trust region policy optimization. In Francis R. Bach and David M. Blei (eds.), *Proceedings of the 32nd International Conference on Machine Learning, ICML 2015, Lille, France, 6-11 July 2015*, volume 37 of *JMLR Workshop and Conference Proceedings*, pp. 1889–1897. JMLR.org, 2015. URL <http://proceedings.mlr.press/v37/schulman15.html>.

John Schulman, Filip Wolski, Prafulla Dhariwal, Alec Radford, and Oleg Klimov. Proximal policy optimization algorithms. *CoRR*, abs/1707.06347, 2017. URL <http://arxiv.org/abs/1707.06347>.

Ryohei Shimizu, Yusuke Mukuta, and Tatsuya Harada. Hyperbolic neural networks++. In *9th International Conference on Learning Representations, ICLR 2021, Virtual Event, Austria, May 3-7, 2021*. OpenReview.net, 2021. URL <https://openreview.net/forum?id=Ec85b0tUwbA>.

David Silver, Aja Huang, Chris J. Maddison, Arthur Guez, Laurent Sifre, George van den Driessche, Julian Schrittwieser, Ioannis Antonoglou, Vedavyas Panneershelvam, Marc Lanctot, Sander Dieleman, Dominik Grewe, John Nham, Nal Kalchbrenner, Ilya Sutskever, Timothy P. Lillicrap, Madeleine Leach, Koray Kavukcuoglu, Thore Graepel, and Demis Hassabis. Mastering the game of go with deep neural networks and tree search. *Nat.*, 529(7587):484–489, 2016. doi: 10.1038/NATURE16961. URL <https://doi.org/10.1038/nature16961>.

Richard S. Sutton and Andrew G. Barto. *Reinforcement learning - an introduction*, 2nd Edition. MIT Press, 2018. URL <http://www.incompleteideas.net/book/the-book-2nd.html>.

Mark Towers, Ariel Kwiatkowski, Jordan K. Terry, John U. Balis, Gianluca De Cola, Tristan Deleu, Manuel Goulão, Andreas Kallinteris, Markus Krimmel, Arjun KG, Rodrigo Perez-Vicente, Andrea Pierré, Sander Schulhoff, Jun Jet Tai, Hannah Tan, and Omar G. Younis. Gymnasium: A standard interface for reinforcement learning environments. *CoRR*, abs/2407.17032, 2024. doi: 10.48550/ARXIV.2407.17032. URL <https://doi.org/10.48550/arXiv.2407.17032>.

Hado van Hasselt, Arthur Guez, and David Silver. Deep reinforcement learning with double q-learning. In Dale Schuurmans and Michael P. Wellman (eds.), *Proceedings of the Thirtieth AAAI Conference on Artificial Intelligence, February 12-17, 2016, Phoenix, Arizona, USA*, pp. 2094–2100. AAAI Press, 2016. doi: 10.1609/AAAI.V30I1.10295. URL <https://doi.org/10.1609/aaai.v30i1.10295>.

Jingjing Xu, Xu Sun, Zhiyuan Zhang, Guangxiang Zhao, and Junyang Lin. Understanding and improving layer normalization. In Hanna M. Wallach, Hugo Larochelle, Alina Beygelzimer, Florence d’Alché-Buc, Emily B. Fox, and Roman Garnett (eds.), *Advances in Neural Information Processing Systems 32: Annual Conference on Neural Information Processing Systems 2019, NeurIPS 2019, December 8-14, 2019, Vancouver, BC, Canada*, pp. 4383–4393, 2019. URL <https://proceedings.neurips.cc/paper/2019/hash/2f4fe03d77724a7217006e5d16728874-Abstract.html>.

Biao Zhang and Rico Sennrich. Root mean square layer normalization. In Hanna M. Wallach, Hugo Larochelle, Alina Beygelzimer, Florence d’Alché-Buc, Emily B. Fox, and Roman Garnett (eds.), *Advances in Neural Information Processing Systems 32: Annual Conference on Neural Information Processing Systems 2019, NeurIPS 2019, December 8-14, 2019, Vancouver, BC, Canada*, pp. 12360–12371, 2019. URL <https://proceedings.neurips.cc/paper/2019/hash/1e8a19426224ca89e83cef47f1e7f53b-Abstract.html>.

# Appendix

Table 1 summarizes the contents of our Appendix:

Table 1: Structure of our appendix.

Appendix Section	Content
Appendix A	Proofs & Derivations
Appendix B	Additional Background for RL and hyperbolic MLR Layers
Appendix C	Environment descriptions
Appendix D	Compute details and hyperparameters
Appendix E	Complete results and additional metrics

## A DERIVATIONS AND PROOFS

This section contains derivations and proofs for the results in

### A.1 POINCARÉ EXPONENTIAL MAP GRADIENTS

We build on the analysis by Guo et al. (2022) and derive the Jacobian of the Poincaré Ball exponential map at the origin.

$$\begin{aligned}
 D\mathbf{x}_H &= \frac{\partial}{\partial \mathbf{x}_E} \exp_0(\mathbf{x}_E) \\
 &= \frac{\partial}{\partial \mathbf{x}_E} \frac{\tanh(\sqrt{c}\|\mathbf{x}_E\|)}{\sqrt{c}\|\mathbf{x}_E\|} \mathbf{x}_E \\
 &= \frac{\tanh(\sqrt{c}\|\mathbf{x}_E\|)}{\sqrt{c}\|\mathbf{x}_E\|} \mathbf{I}_d + \left( \frac{\partial}{\partial \mathbf{x}_E} \frac{\tanh(\sqrt{c}\|\mathbf{x}_E\|)}{\sqrt{c}\|\mathbf{x}_E\|} \right) \mathbf{x}_E,
 \end{aligned} \tag{11}$$

where  $\mathbf{I}_d$  denotes the  $d \times d$  identity matrix.

Deriving the second term yields:

$$\begin{aligned}
 \frac{\partial}{\partial \mathbf{x}_E} \frac{\tanh(\sqrt{c}\|\mathbf{x}_E\|)}{\sqrt{c}\|\mathbf{x}_E\|} &= \frac{\frac{\partial}{\partial \mathbf{x}_E} \tanh(\sqrt{c}\|\mathbf{x}_E\|) \cdot \sqrt{c}\|\mathbf{x}_E\| - \tanh(\sqrt{c}\|\mathbf{x}_E\|) \cdot \frac{\partial}{\partial \mathbf{x}_E} \sqrt{c}\|\mathbf{x}_E\|}{(\sqrt{c}\|\mathbf{x}_E\|)^2} \\
 &\stackrel{(i)}{=} \frac{\operatorname{sech}^2(\sqrt{c}\|\mathbf{x}_E\|) \sqrt{c}\hat{\mathbf{x}}_E \cdot \sqrt{c}\|\mathbf{x}_E\| - \tanh(\sqrt{c}\|\mathbf{x}_E\|) \cdot \sqrt{c}\hat{\mathbf{x}}_E}{c\|\mathbf{x}_E\|^2} \\
 &= \frac{\operatorname{sech}^2(\sqrt{c}\|\mathbf{x}_E\|) c\mathbf{x}_E - \tanh(\sqrt{c}\|\mathbf{x}_E\|) \cdot \sqrt{c}\hat{\mathbf{x}}_E}{c\|\mathbf{x}_E\|^2} \\
 &= \frac{\operatorname{sech}^2(\sqrt{c}\|\mathbf{x}_E\|) \mathbf{x}_E - \tanh(\sqrt{c}\|\mathbf{x}_E\|) \mathbf{x}_E}{\|\mathbf{x}_E\|^2} \\
 &= \left( \frac{\operatorname{sech}^2(\sqrt{c}\|\mathbf{x}_E\|)}{\|\mathbf{x}_E\|^2} - \frac{\tanh(\sqrt{c}\|\mathbf{x}_E\|)}{\sqrt{c}\|\mathbf{x}_E\|^3} \right) \mathbf{x}_E,
 \end{aligned} \tag{12}$$

where we use  $\hat{\mathbf{x}}_E = \frac{\partial}{\partial \mathbf{x}_E} \|\mathbf{x}_E\| = \frac{\mathbf{x}_E}{\|\mathbf{x}_E\|}$  in (i).

Putting Equation 11 and 12 together yields:

$$\frac{\partial}{\partial \mathbf{x}_E} \exp_0(\mathbf{x}_E) = \frac{\tanh(\sqrt{c}\|\mathbf{x}_E\|)}{\sqrt{c}\|\mathbf{x}_E\|} \mathbf{I} + \left( \frac{\operatorname{sech}^2(\sqrt{c}\|\mathbf{x}_E\|)}{\|\mathbf{x}_E\|^2} - \frac{\tanh(\sqrt{c}\|\mathbf{x}_E\|)}{\sqrt{c}\|\mathbf{x}_E\|^3} \right) \frac{\mathbf{x}_E \mathbf{x}_E^\top}{\|\mathbf{x}_E\|^2}. \tag{13}$$

We can see that the Jacobian of the exponential map decays with  $O(\|\mathbf{x}_E\|^{-1})$ , although the important directional term (second summand) can vanish faster with  $O(\|\mathbf{x}_E\|^{-2})$ .

## A.2 HYPERBOLIC NETWORKS++ GRADIENTS

Let us first re-state the forward pass for the hyperbolic networks++ formulation (Shimizu et al., 2021) of the Poincaré multinomial logistic (MLR) layer:

$$v_{\mathbf{z},r}^{\text{HNN++}}(\mathbf{x}_H) = \frac{2\|\mathbf{z}\|}{\sqrt{c}} \sinh^{-1} \left( (1 - \lambda_{\mathbf{x}_H}^c) \sinh(2\sqrt{c}r) + \sqrt{c} \lambda_{\mathbf{x}_H}^c \cosh(2\sqrt{c}r) \langle \hat{\mathbf{z}}, \mathbf{x}_H \rangle \right). \quad (14)$$

Here  $\mathbf{x}_H = \exp_{\bar{0}}(\mathbf{x}_E)$ ,  $\lambda_{\mathbf{x}_H}^c = \frac{2}{1-c\|\mathbf{x}_H\|^2}$  is the conformal factor of the Poincaré Ball,  $\mathbf{z}$  is the weight vector of the layer,  $\hat{\mathbf{z}} = \frac{\mathbf{z}}{\|\mathbf{z}\|}$  are the weights normalized to unit length, and  $r$  a scalar bias term. We omit the class index  $k$  as in the main paper to simplify the notation.

We can re-state Equation 14 as

$$v_{\mathbf{z},r}^{\text{HNN++}}(\mathbf{x}_H) = \frac{2\|\mathbf{z}\|}{\sqrt{c}} \sinh^{-1} (F(\mathbf{x}_H)), \quad (15)$$

with

$$F(\mathbf{x}_H) = (1 - \lambda_{\mathbf{x}_H}^c) \sinh(2\sqrt{c}r) + \sqrt{c} \lambda_{\mathbf{x}_H}^c \cosh(2\sqrt{c}r) \langle \hat{\mathbf{z}}, \mathbf{x}_H \rangle. \quad (16)$$

We first calculate the outer derivative (Equation 15):

$$\nabla_{\mathbf{x}_H} v_{\mathbf{z},r}^{\text{HNN++}}(\mathbf{x}_H) = \frac{2\|\mathbf{z}\|}{\sqrt{c}} \frac{1}{\sqrt{1+F(\mathbf{x}_H)^2}} \nabla_{\mathbf{x}_H} F(\mathbf{x}_H). \quad (17)$$

The gradient of Equation 16  $\nabla_{\mathbf{x}_H} F(\mathbf{x}_H)$  is:

$$\begin{aligned} \nabla_{\mathbf{x}_H} F(\mathbf{x}_H) &= -\sinh(2\sqrt{c}r) \nabla_{\mathbf{x}_H} \lambda_{\mathbf{x}_H}^c + \nabla_{\mathbf{x}_H} \left[ \sqrt{c} \lambda_{\mathbf{x}_H}^c \cosh(2\sqrt{c}r) \langle \hat{\mathbf{z}}, \mathbf{x}_H \rangle \right] \\ &= \sqrt{c} \lambda_{\mathbf{x}_H}^c \cosh(2\sqrt{c}r) \hat{\mathbf{z}} + \left( -\sinh(2\sqrt{c}r) + \sqrt{c} \cosh(2\sqrt{c}r) \langle \hat{\mathbf{z}}, \mathbf{x}_H \rangle \right) \nabla_{\mathbf{x}_H} \lambda_{\mathbf{x}_H}^c \\ &= \frac{2\sqrt{c} \cosh(2\sqrt{c}r)}{1-c\|\mathbf{x}_H\|^2} \hat{\mathbf{z}} + \frac{4c \mathbf{x}_H \left( -\sinh(2\sqrt{c}r) + \sqrt{c} \cosh(2\sqrt{c}r) \langle \hat{\mathbf{z}}, \mathbf{x}_H \rangle \right)}{(1-c\|\mathbf{x}_H\|^2)^2}. \end{aligned} \quad (18)$$

We plug in the definition of the conformal factor  $\lambda_{\mathbf{x}_H}^c = \frac{2}{1-c\|\mathbf{x}_H\|^2}$  and its derivative in the last step.

The term  $\frac{1}{\sqrt{1+F(\mathbf{x}_H)^2}} \leq 1$  in Equation 17 cannot blow up. However, the gradients in Equation 18 grow with  $O((1-c\|\mathbf{x}_H\|^2)^{-2})$  for samples  $\mathbf{x}_H$  close to the boundary of the Poincaré Ball.

## A.3 HYPERBOLOID EXPONENTIAL MAP GRADIENTS

The exponential map of the Hyperboloid at the origin  $\bar{0} = (1/\sqrt{c}, 0, \dots, 0)$  maps a tangent vector  $\mathbf{v} = [0, \mathbf{x}_E] \in T_{\bar{0}}\mathcal{M}$  to the Hyperboloid (Bdeir et al., 2024):

$$\exp_{\bar{0}}(\mathbf{v}) = \frac{1}{\sqrt{c}} \left[ \cosh(\sqrt{c}\|\mathbf{x}_E\|), \sinh(\sqrt{c}\|\mathbf{x}_E\|) \frac{\mathbf{x}_E}{\|\mathbf{x}_E\|} \right]^\top, \quad (19)$$

where the first element is a scalar **time component** and the remaining elements constitute the **space component**.

The derivative of the **time component** is a  $d+1$ -dimensional vector whose first element is zero:

$$\frac{\partial}{\partial \mathbf{v}} \frac{\cosh(\sqrt{c}\|\mathbf{x}_E\|)}{\sqrt{c}} = \left[ 0, \sinh(\sqrt{c}\|\mathbf{x}_E\|) \frac{\mathbf{x}_E}{\|\mathbf{x}_E\|} \right]^\top. \quad (20)$$

For the derivative of the **space component**, we start by reformulating it as:

$$\frac{\partial}{\partial \mathbf{v}} \frac{\sinh(\sqrt{c}\|\mathbf{x}_E\|) \mathbf{x}_E}{\sqrt{c}\|\mathbf{x}_E\|} = \left[ \mathbf{0}, \frac{\partial}{\partial \mathbf{v}} f(\|\mathbf{x}_E\|) \mathbf{x}_E \right] = \left[ \mathbf{0}, f(\|\mathbf{x}_E\|) \mathbf{I}_d + \frac{f'(\|\mathbf{x}_E\|)}{\|\mathbf{x}_E\|} \mathbf{x}_E \mathbf{x}_E^\top \right], \quad (21)$$

where  $f(\|\mathbf{x}_E\|) = \frac{\sinh(\sqrt{c}\|\mathbf{x}_E\|)}{\sqrt{c}\|\mathbf{x}_E\|}$ ,  $\mathbf{I}_d$  is the  $d \times d$  identity matrix, and  $\mathbf{0} \in \mathbb{R}^d$ .

For  $f'(\|\mathbf{x}_E\|)$ , we have:

$$f'(\|\mathbf{x}_E\|) = \frac{\sqrt{c}\|\mathbf{x}_E\| \cosh(\sqrt{c}\|\mathbf{x}_E\|) - \sinh(\sqrt{c}\|\mathbf{x}_E\|)}{\sqrt{c}\|\mathbf{x}_E\|^2}. \quad (22)$$

Plugging Equation 22 into Equation 21 yields:

$$\frac{\sinh(\sqrt{c}\|\mathbf{x}_E\|)}{\sqrt{c}\|\mathbf{x}_E\|} \mathbf{I}_d + \frac{\sqrt{c}\|\mathbf{x}_E\| \cosh(\sqrt{c}\|\mathbf{x}_E\|) - \sinh(\sqrt{c}\|\mathbf{x}_E\|)}{\sqrt{c}\|\mathbf{x}_E\|^3} \mathbf{x}_E \mathbf{x}_E^\top \quad (23)$$

We arrive at the Jacobian of the exponential map by putting Equation 20 and Equation 23 together:

$$\frac{\partial \mathbf{x}_H}{\partial \mathbf{v}} = \frac{\partial}{\partial \mathbf{v}} \exp_{\bar{0}}(\mathbf{v}) = \begin{bmatrix} 0 & \frac{\sinh(\sqrt{c}\|\mathbf{x}_E\|)}{\sqrt{c}\|\mathbf{x}_E\|} \frac{\mathbf{x}_E^\top}{\|\mathbf{x}_E\|} \\ \mathbf{0} & \frac{\sqrt{c}\|\mathbf{x}_E\| \cosh(\sqrt{c}\|\mathbf{x}_E\|) - \sinh(\sqrt{c}\|\mathbf{x}_E\|)}{\sqrt{c}\|\mathbf{x}_E\|^3} \mathbf{x}_E \mathbf{x}_E^\top \end{bmatrix}. \quad (24)$$

#### A.4 PROOFS

*Lemma 4.1.*

$$\begin{aligned} \|f(\mathbf{W}\mathbf{x} + \mathbf{b})\|_2 - \|f(\mathbf{0})\|_2 &\leq \|f(\mathbf{W}\mathbf{x} + \mathbf{b}) - f(\mathbf{0})\|_2 \\ &\stackrel{(i)}{\leq} L\|\mathbf{W}\mathbf{x} + \mathbf{b}\|_2 \\ &\stackrel{(ii)}{\leq} L\|\mathbf{W}\|_2\|\mathbf{x}\|_2 + L\|\mathbf{b}\|_2, \end{aligned}$$

where (i) uses the lipschitz property of  $f$  and (ii) follows from the definition of the induced matrix norm. The special case follows directly by observing that ReLU is 1-Lipschitz with  $\text{ReLU}(0) = 0$ .  $\square$

*Proposition 4.2.* First, we bound the norm of the normalized feature vector. Recall that  $\text{RMS}(\mathbf{x}) = \mathbf{x}/\mu(\mathbf{x})$  with  $\mu(\mathbf{x}) = \sqrt{\varepsilon + \frac{1}{d}\|\mathbf{x}\|_2^2}$ . Then,

$$\|\text{RMS}(\mathbf{x})\|_2^2 = \frac{\|\mathbf{x}\|_2^2}{\varepsilon + \frac{1}{d}\|\mathbf{x}\|_2^2} < \frac{\|\mathbf{x}\|_2^2}{\frac{1}{d}\|\mathbf{x}\|_2^2} = d,$$

and

$$\|\hat{\mathbf{x}}\|_2 = \left\| \frac{1}{\sqrt{d}} f(\text{RMS}(\mathbf{x})) \right\|_2 \stackrel{(i)}{\leq} \frac{1}{\sqrt{d}} (\|f(\mathbf{0})\|_2 + L\|\text{RMS}(\mathbf{x})\|_2) < \frac{1}{\sqrt{d}} \|f(\mathbf{0})\|_2 + L,$$

where (i) follows from Lemma 4.1, conclude the first part.

Second, we bound the conformal factor. Let  $\mathbf{v} = \exp_{\bar{0}}(\hat{\mathbf{x}}) = \tanh(\sqrt{c}\|\hat{\mathbf{x}}\|) \frac{\hat{\mathbf{x}}}{\sqrt{c}\|\hat{\mathbf{x}}\|}$ . We have:

$$\|\mathbf{v}\|_2 = \left\| \tanh(\sqrt{c}\|\hat{\mathbf{x}}\|_2) \frac{\hat{\mathbf{x}}}{\sqrt{c}\|\hat{\mathbf{x}}\|_2} \right\|_2 = \frac{\tanh(\sqrt{c}\|\hat{\mathbf{x}}\|_2)}{\sqrt{c}\|\hat{\mathbf{x}}\|_2} \|\hat{\mathbf{x}}\|_2 = \frac{\tanh(\sqrt{c}\|\hat{\mathbf{x}}\|_2)}{\sqrt{c}}.$$

Applying the previous equality gives

$$\lambda_{\mathbf{v}}^c = \frac{2}{1 - c\|\mathbf{v}\|_2^2} = \frac{2}{1 - \tanh(\sqrt{c}\|\hat{\mathbf{x}}\|_2)^2}$$

which can be further bounded by combining it with the bound on  $\|\hat{\mathbf{x}}\|$  and using the fact that  $\cosh$  is a monotonically increasing function on  $\mathbb{R}_{>0}$ :

$$\lambda_{\mathbf{v}}^c = \frac{2}{1 - \tanh(\sqrt{c}\|\hat{\mathbf{x}}\|_2)^2} = 2 \cosh^2(\sqrt{c}\|\hat{\mathbf{x}}\|) \leq 2 \cosh^2\left(\sqrt{c}\left(\frac{1}{\sqrt{d}}\|f(\mathbf{0})\|_2 + L\right)\right).$$

$\square$

---

## B ADDITIONAL BACKGROUND

### B.1 TRUST-REGION POLICY OPTIMIZATION (TRPO)

TRPO maximizes cumulative reward through gradient ascent on a surrogate objective (Equation equation 25);

$$\begin{aligned} \max_{\theta} \quad & \mathbb{E}_t \left[ \frac{\pi_{\theta}(a_t | s_t)}{\pi_{\theta_{\text{old}}}(a_t | s_t)} A_t^{\pi_{\theta_{\text{old}}}} \right] \\ \text{subject to} \quad & \mathbb{E}_t \left[ D_{\text{KL}}[\pi_{\theta}(a_t | s_t) \| \theta_{\text{old}}] \right] \leq \delta. \end{aligned} \quad (25)$$

Additionally, it enforces an average KL-divergence constraint to keep the new policy close to the data-generating policy. Theoretically, optimizing this objective guarantees monotonic improvement (Schulman et al., 2015). In practice, several approximations are used for deep neural networks. Nevertheless, TRPO tends to retain the monotonic improvement of its theory.

### B.2 DOUBLE DEEP Q-NETWORK

Deep Q Network (DQN) (Mnih et al., 2015) learns the optimal Q-function for discrete action spaces by minimizing a mean-squared error loss against an off-policy bootstrap target while reusing replayed transitions. The standard target is  $Q_{\text{tar:DQN}}^{\pi}(s, a) = r + \gamma \max_{a'} Q^{\pi}(s', a')$ , which, together with experience replay and a periodically updated target network, stabilizes training. However, because the same function approximator effectively selects both the maximizing action and evaluates its value under noise and approximation error, the max operator induces systematic overestimation bias (Sutton & Barto, 2018).

Double DQN (DDQN) (van Hasselt et al., 2016) reduces the overestimation bias that arises when the same network both selects and evaluates the maximized next-state value. DDQN uses the online network with parameters  $\theta$  to select the greedy next action, and a target network with parameters  $\varphi$  to evaluate that action when calculating the TD target:  $Q_{\text{tar:DDQN}}^{\pi}(s, a) = r + \gamma Q_{\varphi}^{\pi}(s', \arg \max_{a'} Q_{\theta}^{\pi}(s', a'))$ . This decorrelates action selection from evaluation, effectively mitigating overestimation bias.

### B.3 HYPERBOLIC MULTINOMIAL LOGISTIC REGRESSION

Multinomial Logistic Regression (MLR) in hyperbolic space  $\mathcal{M}$  is defined as the log-linear model with parameters  $\mathbf{z}_k \in \mathbb{R}^d$ ,  $r_k \in \mathbb{R}$  that predicts the probability  $p(\mathbf{y} = k | \mathbf{x})$  of an input  $\mathbf{x} \in \mathcal{M} \simeq \mathbb{R}^d$  belonging to a specific class  $k \in \{1, \dots, K\}$ :

$$p(\mathbf{y} = k | \mathbf{x}) \propto \exp(v_{\mathbf{z}_k, r_k}(\mathbf{x})), \quad v_{\mathbf{z}_k, r_k}(\mathbf{x}) = \|\mathbf{z}_k\|_{\mathcal{T}_{\mathbf{p}_k} \mathcal{M}} d_{\mathcal{M}}(\mathbf{x}, \mathcal{H}_{\mathbf{z}_k, r_k}).$$

Here,  $\exp(v_{\mathbf{z}_k, r_k}(\mathbf{x}))$  is the logit for class  $k$  and  $v_{\mathbf{z}_k, r_k}(\mathbf{x})$  the signed distance to the margin hyperplane  $\mathcal{H}_{\mathbf{z}_k, r_k}$ . To prevent over-parametrization, each hyperplane is characterized by aligning its normal vector  $\mathbf{a}_k$  and shift  $\mathbf{p}_k$ , requiring only  $d + 1$ -parameters per hyperplane (Shimizu et al., 2021; Bdeir et al., 2024). To leverage established Euclidean optimization algorithms, all parameters are maintained in Euclidean space and mapped to their hyperbolic counterparts. The normal vector  $\mathbf{a}_k \in \mathcal{T}_{\mathbf{p}_k} \mathcal{M}$  is obtained by parallel transporting the Euclidean parameter  $\mathbf{z}_k \in \mathbb{R}^d$  to the origin  $\bar{0}$ :  $\mathbf{a}_k = PT_{\bar{0} \rightarrow \mathbf{p}}(\mathbf{z}_k)$  with  $\mathbf{z}_k \in \mathcal{T}_{\bar{0}} \mathcal{M}$ . The hyperplane's shift  $\mathbf{p}_k \in \mathcal{M}$  is defined as scalar multiple of the same unit tangent vector  $\mathbf{p}_k = \exp_{\bar{0}} \left( \frac{r_k}{\|\mathbf{z}_k\|} \mathbf{z}_k \right)$  with  $r_k \in \mathbb{R}$ .

---

### B.3.1 POINCARÉ BALL MLR

For the Poincaré Ball we have:

$$\begin{aligned}
\mathbf{p}_k &= \exp_{\bar{0}} \left( \frac{r_k}{\|\mathbf{z}_k\|} \mathbf{z}_k \right) = \frac{\tanh(\sqrt{c} r_k)}{\sqrt{c} \|\mathbf{z}_k\|} \mathbf{z}_k, \\
\mathbf{a}_k &= PT_{\bar{0} \rightarrow \mathbf{p}}(\mathbf{z}_k) = (1 - \tanh^2(\sqrt{c} r_k)) \mathbf{z}_k, \\
\mathcal{H}_{\mathbf{z}_k, r_k} &= \mathcal{H}_{\mathbf{a}_k, \mathbf{p}_k} = \{ \mathbf{x} \in \mathbb{P}_c^d : \langle \mathbf{a}_k, \ominus \mathbf{p}_k \oplus \mathbf{x} \rangle = 0 \}, \\
d_{\mathbb{P}_c^d}(\mathbf{x}, \mathcal{H}_{\mathbf{z}_k, r_k}) &= d_{\mathbb{P}}(\mathbf{x}, \mathcal{H}_{\mathbf{a}_k, \mathbf{p}_k}) = \frac{1}{\sqrt{c}} \sinh^{-1} \left( \frac{2\sqrt{c} |\langle \mathbf{a}_k, \ominus \mathbf{p}_k \oplus \mathbf{x} \rangle|}{(1 - c \|\ominus \mathbf{p}_k \oplus \mathbf{x}\|^2) \|\mathbf{a}_k\|} \right),
\end{aligned}$$

where  $\ominus$  and  $\oplus$  denote the Möbius addition and subtraction (Ganea et al., 2018). The Poincaré Ball MLR layer (Shimizu et al., 2021) can then be summarized as

$$v_{\mathbf{z}_k, r_k}^{\text{HNN++}}(\mathbf{x}) = \frac{2 \|\mathbf{z}_k\|}{\sqrt{c}} \sinh^{-1} \left( (1 - \lambda_{\mathbf{x}}^c) \sinh(2\sqrt{c} r_k) + \sqrt{c} \lambda_{\mathbf{x}}^c \cosh(2\sqrt{c} r_k) \left\langle \frac{\mathbf{z}_k}{\|\mathbf{z}_k\|}, \mathbf{x} \right\rangle \right).$$

### B.3.2 HYPERBOLOID MLR

For the Hyperboloid, the tangent vectors  $\mathbf{z}_k$  are represented in  $\mathbb{R}^d$  rather than the full  $\mathbb{R}^{d+1}$  space that would typically characterize tangent vectors at the origin of the Hyperboloid. However, to preserve the correct number of degrees of freedom, we omit the time component, which is constrained to be zero. That said, we have:

$$\begin{aligned}
\mathbf{p}_k &= \exp_{\bar{0}} \left( \frac{r_k}{\|\mathbf{z}_k\|} \mathbf{z}_k \right) = \frac{1}{\sqrt{c}} \left[ \cosh(\sqrt{c} r_k), \sinh(\sqrt{c} r_k) \frac{\mathbf{z}_k}{\|\mathbf{z}_k\|} \right]^\top \\
\mathbf{a}_k &= PT_{\bar{0} \rightarrow \mathbf{p}}(\mathbf{z}_k) = \left[ \sinh(\sqrt{c} r_k) \|\mathbf{z}_k\|, \cosh(\sqrt{c} r_k) \mathbf{z}_k \right]^\top, \\
\mathcal{H}_{\mathbf{z}_k, r_k} &= \mathcal{H}_{\mathbf{a}_k, \mathbf{p}_k} = \{ \mathbf{x} \in \mathbb{H}_c^d : \langle \mathbf{a}_k, \mathbf{x} \rangle_{\mathcal{L}} = 0 \}, \\
d_{\mathbb{H}_c^d}(\mathbf{x}, \mathcal{H}_{\mathbf{z}_k, r_k}) &= \frac{1}{\sqrt{c}} \sinh^{-1} \left( \frac{\sqrt{c}}{\|\mathbf{z}_k\|} (-x_0 \sinh(\sqrt{c} r_k) \|\mathbf{z}_k\| + \cosh(\sqrt{c} r_k) \langle \mathbf{z}_k, \mathbf{x}_s \rangle) \right).
\end{aligned}$$

The Hyperboloid MLR layer (Bdeir et al., 2024) can then be summarized as

$$v_{\mathbf{z}_k, r_k}^{\text{HB}}(\mathbf{x}) = \frac{\|\mathbf{z}_k\|}{\sqrt{c}} \sinh^{-1} \left( \frac{\sqrt{c}}{\|\mathbf{z}_k\|} (-x_0 \sinh(\sqrt{c} r_k) \|\mathbf{z}_k\| + \cosh(\sqrt{c} r_k) \langle \mathbf{z}_k, \mathbf{x}_s \rangle) \right), \quad (26)$$

where  $\mathbf{x}_s = (x_1, \dots, x_d)$  denotes the *space component* and  $x_0$  the *time component*.

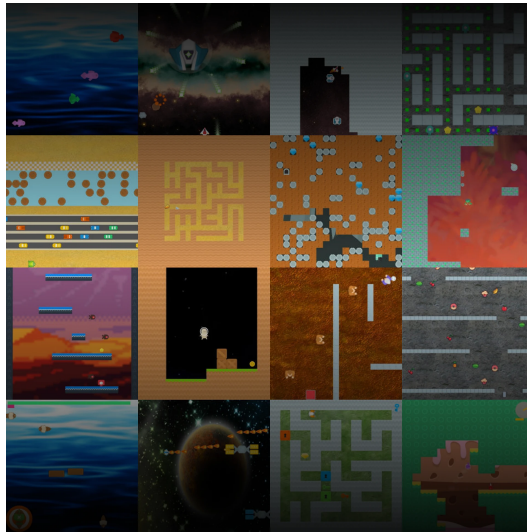


Figure 10: Visualization of all ProcGen environments.

## C ENVIRONMENTS

In this Section, we review the environments used in our paper and discuss evaluation differences to existing methods.

### C.1 PROCGEN

ProcGen (Cobbe et al., 2020) uses RGB frames of size  $64 \times 64 \times 3$  as observations. We visualize the 16 games in Figure 10. The action space is discrete with 15 actions. For training, we follow the protocol by (Cetin et al., 2023): fix difficulty to “easy” and train on the first 200 levels (seeds 0–199). For testing, we evaluate on all levels of the easy distribution. For the table, we run a single end-of-training evaluation on 100 parallel environments sampled from the train and test distribution, respectively. We then normalize the scores for each individual run before aggregating.

### C.2 ATARI

The Arcade Learning Environment (Bellemare et al., 2015; Towers et al., 2024) provides a standardized interface for deep RL research based on dozens of Atari 2600 games. Of these, 57 are commonly used in evaluation. The observations are RGB frames  $210 \times 160 \times 3$ , which are preprocessed via grayscaling, downsampling to  $84 \times 84$ , and frame stacking. The action space consists of up to 18 discrete joystick/button combinations, with most games using a subset and action repeat (frame skipping) to help with jittering. The rewards are clipped to  $\{-1, 0, +1\}$ . As the game dynamics are naturally deterministic, the benchmark uses randomized no-op resets as outlined in the original DQN paper (Mnih et al., 2015) and cleanRL (Huang et al., 2022).

### C.3 EVALUATION DIFFERENCES WITH EXISTING WORKS

Our paper builds on the seminal work by Cetin et al. (2023). However, we struggled to reproduce their results, which we believe is mainly due to three reasons. First, their source code does not use seeding. As deep RL is notoriously seed-dependent (Henderson et al., 2018; Agarwal et al., 2021), we find exact reproduction impossible. Second, we use a different implementation for the mathematical operations of hyperbolic geometry, which possibly affects the results. This issue is known within the hyperbolic deep learning community (Katsman & Gilbert, 2025). Third, we use different versions of PyTorch and Python. Additionally, our evaluation follows a slightly different protocol (see Appendix C.1), and we use Pytorch’s evaluation mode before generating results for our agents. We hope that by releasing our complete code, we can take a step towards more reproducible research in hyperbolic deep RL.

---

Table 2: **Wall-clock results.**

	ProcGen forward	NameThisGame
<b>Euclidean</b>	14ms	17h52m
<b>Hyper+S-RYM</b> (Cetin et al., 2023)	19.3ms	58h21m
<b>HYPER++</b>	14.7ms	35h25m

## D EXPERIMENTAL DETAILS

### D.1 HARDWARE & RUNTIME

For our experiments, we used Nvidia A100 GPUs. For ProcGen, we can train up to four agents in parallel on a single GPU with 40GB. We report wall-clock times for forward passes on ProcGen and for full runs on NameThisGame in Table 2. Note that agent performance can be a confounding factor for results when timing on full experiments because agent performance can either be positively or negatively correlated with episode length. For NameThisGame, e.g., better agents generate longer episodes. We average over 100 passes for the forward pass results and five seeds for the NameThisGame results.

### D.2 NETWORK ARCHITECTURE

For ProcGen, we use the same Impala-ResNet (Espeholt et al., 2018) as (Cetin et al., 2023), which we visualize in Figure 11. Our modifications are shaded in purple. They consist of

1. using RMSNorm (Zhang & Sennrich, 2019) before scaling the Euclidean features,
2. using TanH instead of ReLU as penultimate activation,
3. applying learned feature scaling before the exponential map, and
4. using the Hyperboloid instead of the Poincaré Ball.

For Atari, we use the NatureCNN (Mnih et al., 2015) architecture with the same modifications applied as for ProcGen.

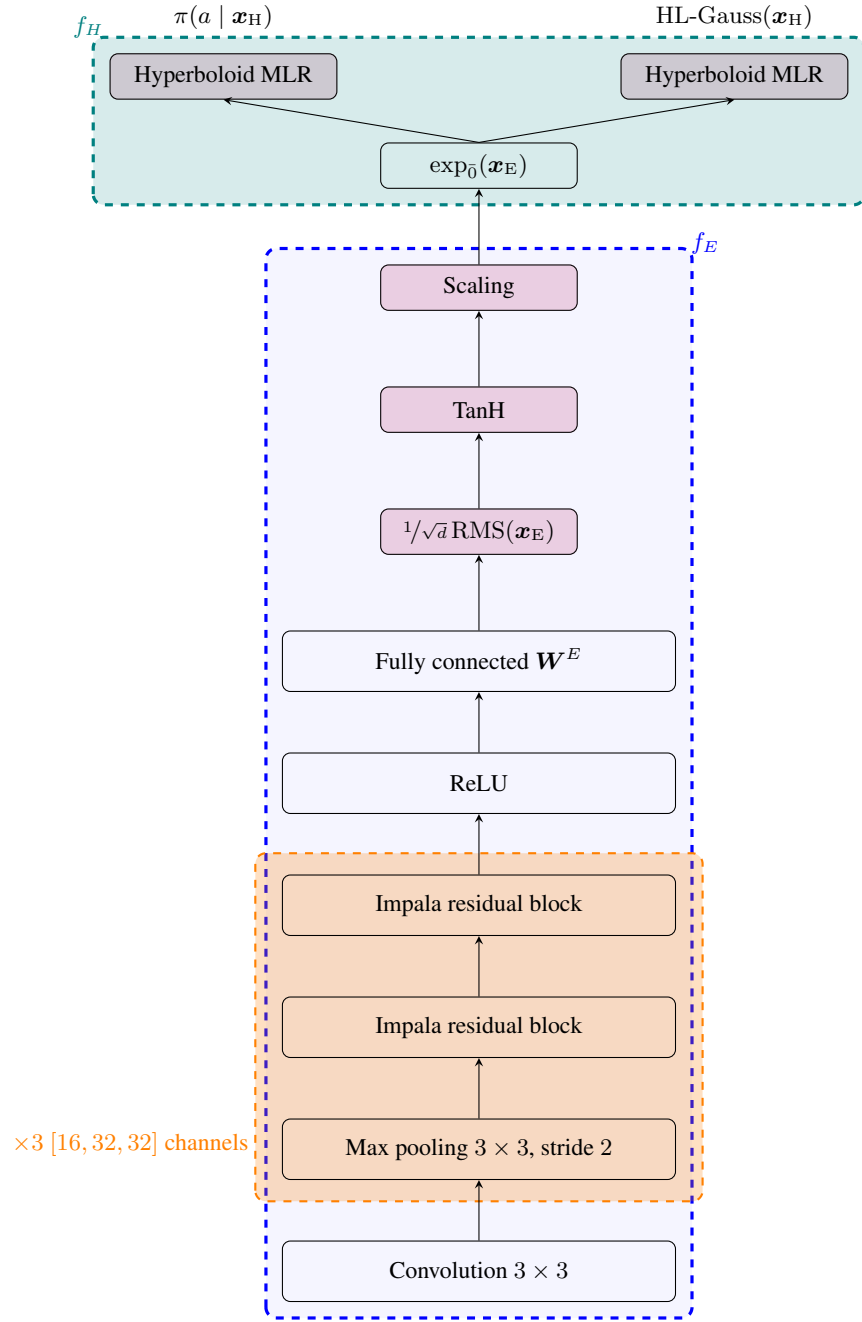


Figure 11: **Hybrid neural network architecture.**  $f_H$  denotes hyperbolic layers,  $f_E$  Euclidean layers. Components that are specific to HYPER++ are shaded in purple.

---

Table 4: PPO hyperparameters for ProcGen.

PPO hyperparameters	
Parallel environments	64
Stacked input frames	1
Steps per rollout	16384
Training epochs per rollout	3
Batch size	2048
Normalize rewards	True
Discount $\gamma$	0.999
GAE $\lambda$ (Schulman et al., 2015)	0.95
PPO clipping	0.2
Entropy coefficient	0.01
Value coefficient	0.5
Shared network	True
Impala stack filter sizes	16, 32, 32
Default latent representation size	32
Optimizer	Adam (Kingma & Ba, 2015)
Optimizer learning rate	$5 \times 10^{-4}$
Optimizer stabilization constant ( $\epsilon$ )	$1 \times 10^{-5}$
Maximum gradient norm.	0.5

Table 5: DDQN hyperparameters for Atari.

Atari hyperparameters	
Environment steps	10M
Discount $\gamma$	0.99
$\epsilon$ start	1
$\epsilon$ end	0.01
Exploration fraction	10% of steps
Replay buffer size	1M
Target network update frequency	1000
Default latent representation size	512
Batch size	32
Training frequency	4
Optimizer	Adam (Kingma & Ba, 2015)
Optimizer learning rate	$1 \times 10^{-4}$
Optimizer stabilization constant ( $\epsilon$ )	$2.5 \times 10^{-5}$

### D.3 HYPERPARAMETERS

We specify the hyperparameters for all PPO agents in Table 4 and for the DDQN agents in Table 5. For DDQN, we use the hyperparameters and preprocessing steps from cleanRL (Huang et al., 2022). Additional parameters for our method are in Table 5. On ProcGen, our agent uses a latent dimension  $d = 64$  compared to  $d = 32$  for Hyper+S-RYM. For HL-Gauss (Imani & White, 2018), we use the default parameters specified by Farebrother et al. (2024). We set the learned scaling hyperparameter to  $\alpha = 0.95$  without tuning for all experiments. When using RMSNorm or LayerNorm, we do not use affine parameters, because they can overfit (Xu et al., 2019) to the training set.

Table 3: HYPER++ hyperparameters.

HYPER++	
Loss: Number of bins	51
Loss: Min clip	-10.0
Loss: Max clip	+10.0
Last Euclidean Activation	TanH
Learned scaling $\alpha$	0.95

## E ADDITIONAL RESULTS

### E.1 FULL TRAIN RESULTS

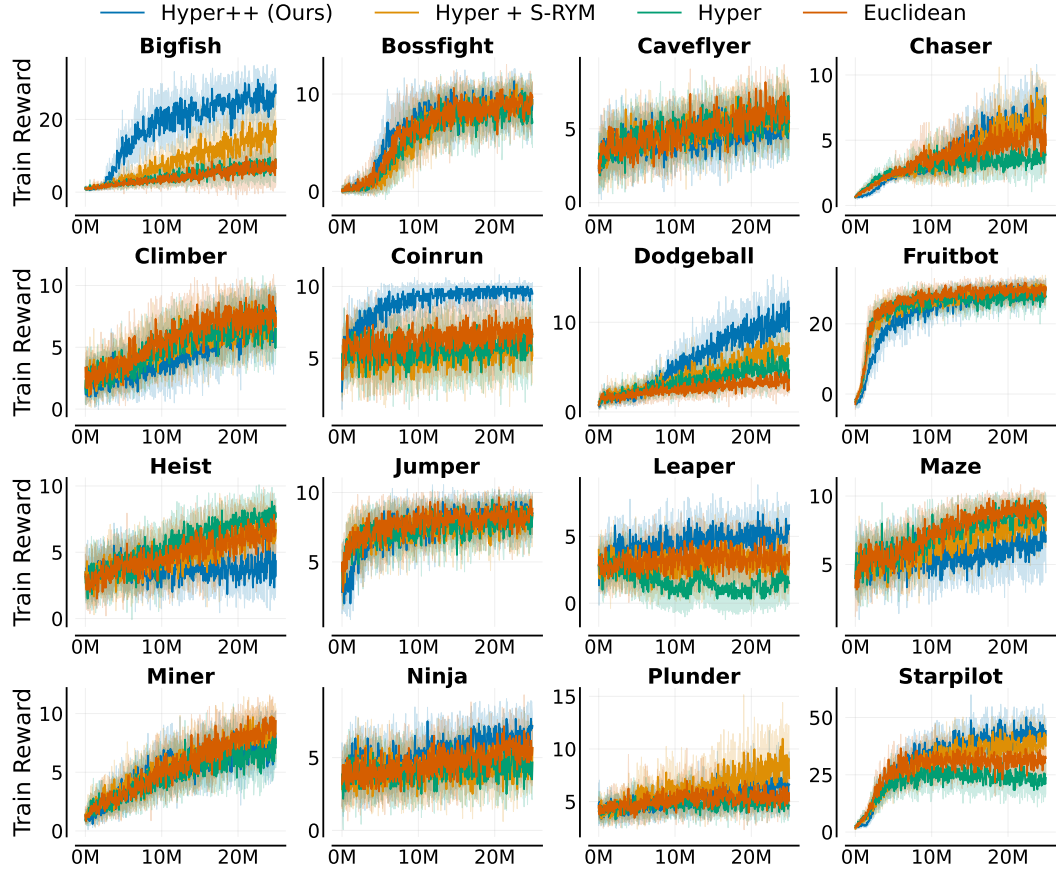


Figure 12: ProcGen Train Learning curves.

Table 6: ProcGen Train Results (mean  $\pm$  std).

	Hyper	Euclidean	Hyper + S-RYM	Hyper++ (Ours)
<b>bigfish</b>	$7.12 \pm 1.7$	$7.81 \pm 5.0$	$17.38 \pm 3.3$	<b><math>25.66 \pm 2.8</math></b>
<b>starpilot</b>	$20.43 \pm 1.5$	$31.14 \pm 4.4$	$38.92 \pm 1.9$	<b><math>43.43 \pm 3.7</math></b>
<b>dodgeball</b>	$5.42 \pm 0.9$	$3.28 \pm 0.7$	$6.26 \pm 0.7$	<b><math>10.28 \pm 1.0</math></b>
<b>coinrun</b>	$6.25 \pm 1.4$	$7.37 \pm 1.2$	$5.53 \pm 1.0$	<b><math>9.67 \pm 0.2</math></b>
<b>leaper</b>	$1.65 \pm 1.5$	$3.35 \pm 1.0$	$3.23 \pm 2.0$	<b><math>5.25 \pm 0.9</math></b>
<b>ninja</b>	$4.63 \pm 0.8$	$5.65 \pm 0.9$	$4.37 \pm 0.5$	<b><math>6.67 \pm 0.6</math></b>
<b>fruitbot</b>	$27.09 \pm 0.9$	$29.40 \pm 0.8$	$29.36 \pm 0.7$	<b><math>29.89 \pm 0.4</math></b>
<b>jumper</b>	$8.27 \pm 0.3$	$8.17 \pm 0.6$	$8.17 \pm 0.7$	<b><math>8.53 \pm 0.3</math></b>
<b>bossfight</b>	$8.49 \pm 0.7$	<b><math>9.40 \pm 0.5</math></b>	$9.38 \pm 0.7$	$9.27 \pm 0.7$
<b>miner</b>	$6.86 \pm 0.5$	$8.52 \pm 0.8$	<b><math>8.53 \pm 1.0</math></b>	$8.10 \pm 1.4$
<b>chaser</b>	$3.85 \pm 0.5$	$5.04 \pm 0.9$	<b><math>7.60 \pm 0.8</math></b>	$7.12 \pm 0.9$
<b>climber</b>	$6.72 \pm 0.7$	<b><math>7.79 \pm 0.5</math></b>	$7.43 \pm 0.8$	$7.27 \pm 0.7$
<b>caveflyer</b>	$5.81 \pm 0.5$	<b><math>6.41 \pm 0.3</math></b>	$6.13 \pm 0.6$	$5.04 \pm 0.6$
<b>maze</b>	<b><math>8.88 \pm 0.5</math></b>	$8.88 \pm 0.7$	$7.80 \pm 0.8$	$6.90 \pm 1.4$
<b>plunder</b>	$4.99 \pm 0.9$	$5.30 \pm 0.5$	<b><math>8.81 \pm 1.5</math></b>	$6.23 \pm 0.9$
<b>heist</b>	<b><math>7.57 \pm 0.6</math></b>	$6.78 \pm 1.2$	$6.68 \pm 0.8$	$3.95 \pm 1.5$

## E.2 FULL TEST RESULTS

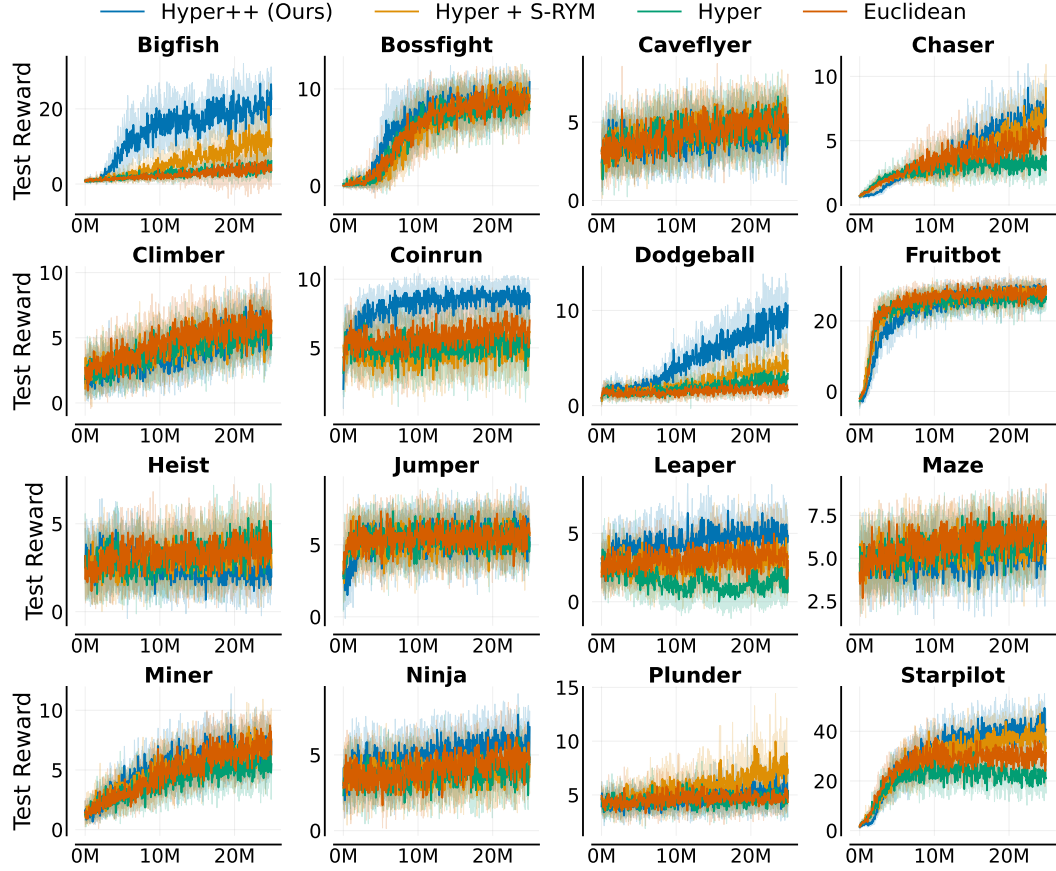


Figure 13: ProcGen Learning curves.

Table 7: ProcGen Test Results (mean  $\pm$  std).

	Hyper	Euclidean	Hyper + S-RYM	Hyper++ (Ours)
<b>bigfish</b>	$4.80 \pm 1.9$	$3.60 \pm 3.4$	$11.88 \pm 2.7$	<b><math>20.01 \pm 4.8</math></b>
<b>starpilot</b>	$22.21 \pm 4.0$	$30.44 \pm 3.1$	$35.59 \pm 2.8$	<b><math>42.49 \pm 2.6</math></b>
<b>dodgeball</b>	$2.38 \pm 0.2$	$1.79 \pm 0.3$	$3.95 \pm 0.8$	<b><math>9.41 \pm 1.2</math></b>
<b>coinrun</b>	$5.07 \pm 1.3$	$6.13 \pm 1.2$	$5.57 \pm 1.1$	<b><math>8.72 \pm 0.4</math></b>
<b>leaper</b>	$1.38 \pm 1.4$	$3.58 \pm 1.3$	$3.33 \pm 2.0$	<b><math>5.13 \pm 1.0</math></b>
<b>ninja</b>	$4.08 \pm 0.5$	$4.65 \pm 0.5$	$4.27 \pm 0.4$	<b><math>5.68 \pm 0.4</math></b>
<b>chaser</b>	$3.34 \pm 0.6$	$4.55 \pm 1.0$	$6.67 \pm 0.7$	<b><math>7.27 \pm 0.9</math></b>
<b>miner</b>	$5.78 \pm 1.1$	$7.15 \pm 0.6$	$7.07 \pm 1.1$	<b><math>7.21 \pm 0.7</math></b>
<b>jumper</b>	$5.28 \pm 0.6$	$5.08 \pm 0.5$	$5.28 \pm 0.4$	<b><math>5.30 \pm 0.4</math></b>
<b>climber</b>	$5.41 \pm 0.7$	<b><math>5.89 \pm 0.7</math></b>	$5.52 \pm 0.9$	$5.86 \pm 1.2$
<b>bossfight</b>	$8.50 \pm 0.7$	<b><math>9.50 \pm 0.8</math></b>	$9.03 \pm 0.8$	$9.40 \pm 0.7$
<b>fruitbot</b>	$26.37 \pm 2.0$	$27.88 \pm 0.7$	<b><math>28.44 \pm 0.5</math></b>	$28.28 \pm 0.9$
<b>caveflyer</b>	$4.91 \pm 0.5$	<b><math>5.22 \pm 0.3</math></b>	$4.83 \pm 0.5$	$4.12 \pm 0.4$
<b>maze</b>	$6.38 \pm 0.6$	<b><math>6.43 \pm 0.5</math></b>	$5.85 \pm 0.3$	$5.17 \pm 0.8$
<b>heist</b>	$3.58 \pm 0.5$	<b><math>3.68 \pm 0.5</math></b>	$3.38 \pm 0.5$	$2.28 \pm 1.0$
<b>plunder</b>	$4.58 \pm 0.7$	$4.71 \pm 0.5$	<b><math>7.45 \pm 0.7</math></b>	$5.82 \pm 1.6$

### E.3 ADDITIONAL ABLATION METRICS

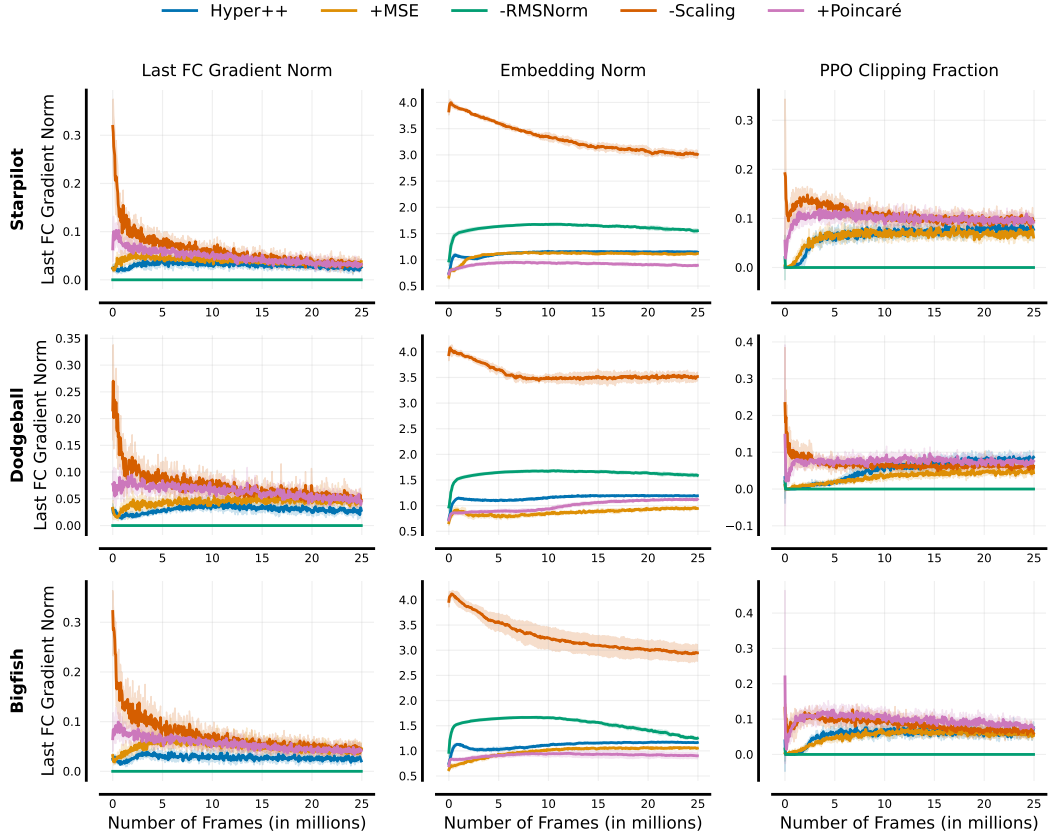


Figure 14: **Additional training metrics of hyperbolic deep RL agents.** Agents w/o RMSNorm (Zhang & Sennrich, 2019) (–RMSNorm) suffer from growing embedding norms and vanishing gradients in the encoder. Using MSE instead of HL-Gauss (Imani & White, 2018) (+MSE) leads to larger initial encoder gradients due to gradients scaling proportional to the loss for MSE. Not using learned feature scaling (–Scaling) has the largest embedding norms and gradients, which are quickly compensated by RMSNorm’s gradient variance normalization (Zhang & Sennrich, 2019).

### E.4 GRADIENT AND LOSS VARIANCE ANALYSIS

Figure 15 shows the evolution of the loss and the loss variance over the course of the training, averaged over all runs. Compared to MSE, the categorical loss is both higher and has higher variance. However, our paper argues that *not the loss values matter, but the gradients instead*. Table 8 shows the L1 and L2 gradient norms of the penultimate layer (last FC layer in the encoder) using the final 25% of training steps. Despite higher loss values and variance, using the HL-Gauss loss yields smaller, lower-variance gradients.

Table 8: **Penultimate layer layer gradient statistics.**

Agent	L2 Grad Norm	L1 Grad Norm	N_runs
Euclidean	$0.0788 \pm 0.0276$	$0.0506 \pm 0.0256$	96
Euclidean+Categorical	$0.0695 \pm 0.0228$	$0.0460 \pm 0.0240$	96
Hyper++	$0.0258 \pm 0.0099$	$0.0294 \pm 0.0155$	96
Hyper++-mse	$0.0327 \pm 0.0102$	$0.0346 \pm 0.0134$	96

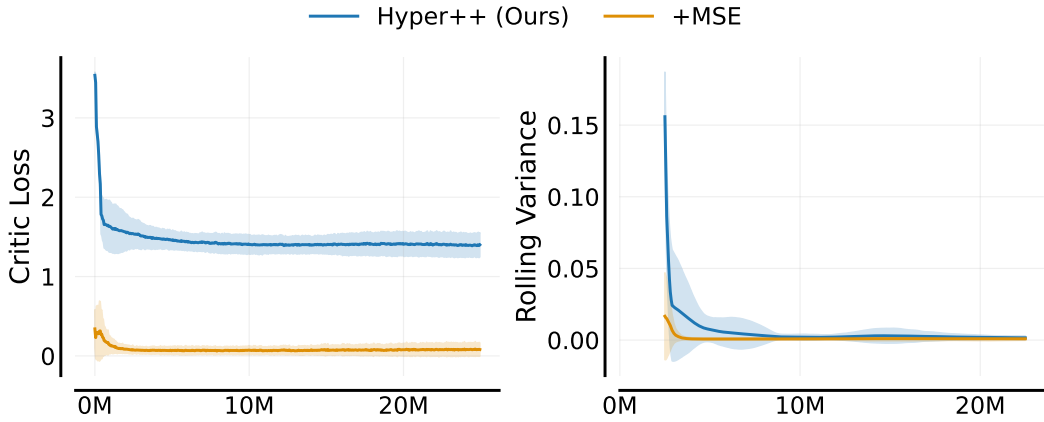


Figure 15: **Critic loss and variance.** We plot the critic loss and variance for our method when using MSE and the categorical loss, averaged over all runs and environments. The categorical HL-Gauss loss (Imani & White, 2018) has higher loss values and variance than MSE.

### E.5 LEARNING CURVES FOR ATARI GAMES

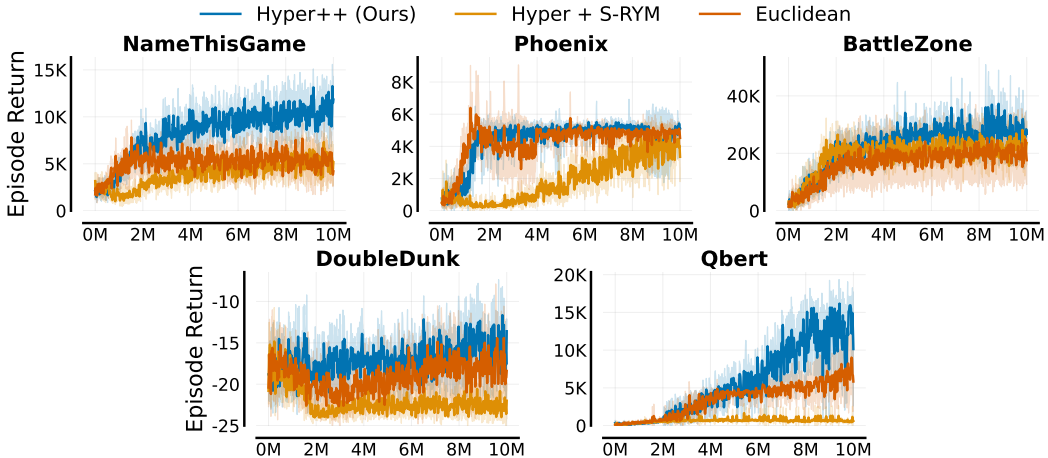


Figure 16: **Atari-5 learning curves.** HYPER++ outperforms the baselines on all environments with particularly strong gains in NAMETHISGAME and QBERT. RESULTS ARE AVERAGED OVER FIVE SEEDS.

## E.6 POLYAK AVERAGING EXPERIMENT

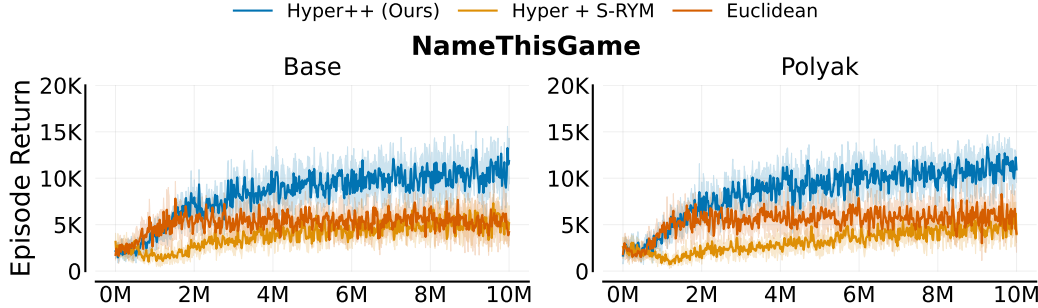


Figure 17: **Polyak averaging (NAMETHISGAME).** Polyak averaging refers to exponential moving average updates for the target network instead of hard replacement updates. Algorithm performance is not meaningfully affected by the form of the target network update. Runs are averaged over five seeds, with one standard deviation as error.

## E.7 OFF-BATCH PPO METRICS

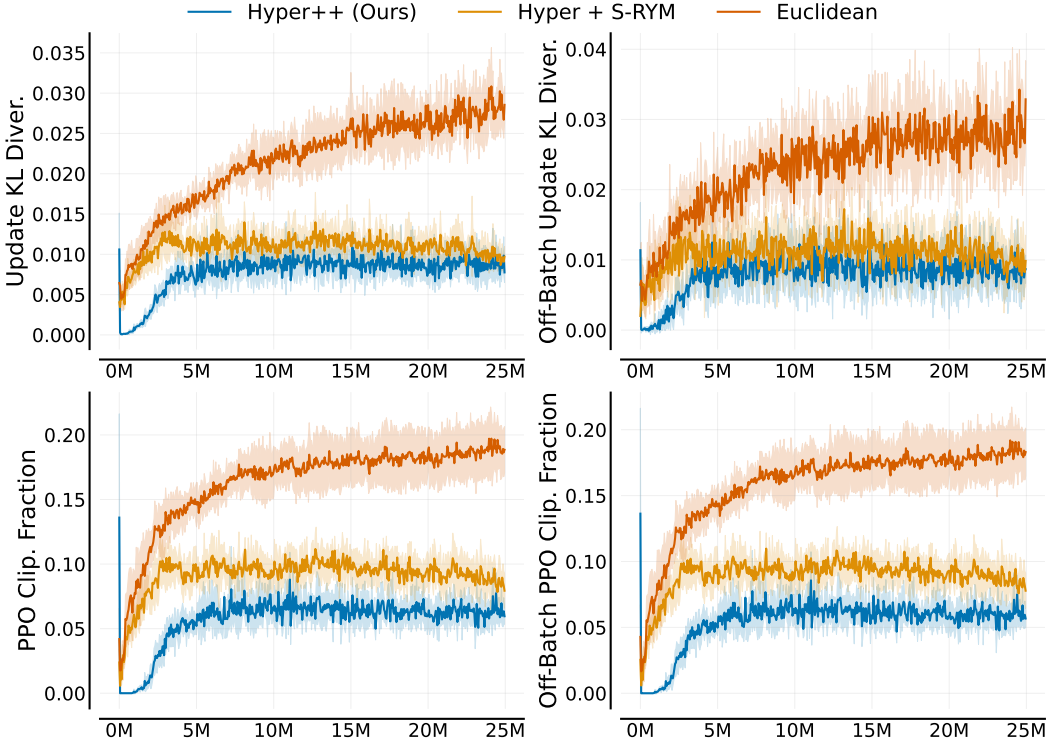


Figure 18: **Off-batch PPO stability metrics.** We track the update KL divergence and PPO clipping fraction for the batch that has currently been updated (left column) and for a batch of randomly sampled on-policy states (right column). The figures show a high level of similarity for the evolution of both metrics. For off-batch data, the update KL divergence has a noticeably higher variance.

---

## E.8 FULL ABLATION RESULTS

Table 9: ProcGen ablation Train results (mean  $\pm$  std).

	Ours	Ours+Poinc.	Ours w/o Scaling	Ours+MSE	Ours+C51	Ours w/o RMS	Ours+SN (Full)	Ours+SN (Penult.)	Euc.+RMS	Euc.+HL-Gauss	Ours+Euc.
<b>bigfish</b>	<b>27.02<math>\pm</math>1.9</b>	17.35 $\pm$ 4.0	20.28 $\pm$ 3.1	21.72 $\pm$ 4.3	19.93 $\pm$ 3.3	1.04 $\pm$ 0.2	0.94 $\pm$ 0.1	1.04 $\pm$ 0.2	5.95 $\pm$ 4.7	11.59 $\pm$ 3.8	24.87 $\pm$ 1.6
<b>dodgeball</b>	<b>10.46<math>\pm</math>1.0</b>	8.15 $\pm$ 1.0	8.12 $\pm$ 0.5	8.06 $\pm$ 1.5	7.95 $\pm$ 1.4	1.86 $\pm$ 0.3	1.64 $\pm$ 0.3	1.73 $\pm$ 0.1	5.08 $\pm$ 1.0	4.63 $\pm$ 1.5	9.72 $\pm$ 1.3
<b>leaper</b>	<b>4.87<math>\pm</math>0.7</b>	3.47 $\pm$ 0.9	3.83 $\pm$ 0.8	2.80 $\pm$ 0.5	4.22 $\pm$ 1.2	3.57 $\pm$ 0.6	3.57 $\pm$ 0.4	3.35 $\pm$ 0.3	3.33 $\pm$ 1.1	4.13 $\pm$ 0.9	4.38 $\pm$ 1.0
<b>coinrun</b>	<b>9.68<math>\pm</math>0.2</b>	9.52 $\pm$ 0.1	9.48 $\pm$ 0.3	8.22 $\pm$ 0.3	9.55 $\pm$ 0.2	5.68 $\pm$ 0.2	5.78 $\pm$ 0.4	6.07 $\pm$ 0.2	8.45 $\pm$ 1.4	9.27 $\pm$ 0.2	9.55 $\pm$ 0.2
<b>fruitbot</b>	<b>30.13<math>\pm</math>1.2</b>	29.89 $\pm$ 0.6	30.04 $\pm$ 0.8	29.83 $\pm$ 1.3	27.23 $\pm$ 0.9	-1.49 $\pm$ 0.3	-1.82 $\pm$ 0.3	-1.54 $\pm$ 0.2	28.08 $\pm$ 1.1	29.70 $\pm$ 1.7	27.49 $\pm$ 0.9
<b>bossfight</b>	9.55 $\pm$ 0.9	9.36 $\pm$ 1.2	8.86 $\pm$ 0.7	<b>9.94<math>\pm</math>0.4</b>	8.62 $\pm$ 0.6	0.48 $\pm$ 0.2	0.48 $\pm$ 0.2	0.43 $\pm$ 0.3	9.14 $\pm$ 0.5	6.46 $\pm$ 1.2	8.29 $\pm$ 0.6
<b>miner</b>	7.49 $\pm$ 0.6	<b>7.93<math>\pm</math>0.8</b>	7.22 $\pm$ 1.2	7.32 $\pm$ 1.2	4.53 $\pm$ 1.5	1.54 $\pm$ 0.4	1.43 $\pm$ 0.3	1.27 $\pm$ 0.2	6.09 $\pm$ 2.5	4.65 $\pm$ 2.0	6.68 $\pm$ 1.0
<b>ninja</b>	5.90 $\pm$ 0.7	<b>6.45<math>\pm</math>0.9</b>	5.62 $\pm$ 0.7	5.27 $\pm$ 0.6	5.13 $\pm$ 0.9	3.43 $\pm$ 0.4	3.17 $\pm$ 0.6	3.32 $\pm$ 0.5	5.95 $\pm$ 0.3	4.32 $\pm$ 0.3	5.07 $\pm$ 0.4
<b>jumper</b>	8.20 $\pm$ 0.3	8.68 $\pm$ 0.4	8.57 $\pm$ 0.3	<b>8.87<math>\pm</math>0.3</b>	7.75 $\pm$ 0.4	3.08 $\pm$ 0.6	3.05 $\pm$ 0.7	3.10 $\pm$ 0.3	8.57 $\pm$ 0.3	7.55 $\pm$ 1.4	8.37 $\pm$ 0.6
<b>cavefever</b>	4.85 $\pm$ 0.5	5.05 $\pm$ 0.4	5.29 $\pm$ 0.3	<b>5.97<math>\pm</math>0.8</b>	4.27 $\pm$ 0.4	3.45 $\pm$ 0.5	3.87 $\pm$ 0.4	3.97 $\pm$ 0.5	4.44 $\pm$ 0.3	4.81 $\pm$ 0.3	
<b>climber</b>	6.52 $\pm$ 0.6	5.00 $\pm$ 1.4	7.65 $\pm$ 0.2	3.39 $\pm$ 0.8	2.63 $\pm$ 0.2	2.63 $\pm$ 0.2	2.16 $\pm$ 0.4	7.64 $\pm$ 0.8	6.11 $\pm$ 1.4	6.58 $\pm$ 0.6	
<b>starpilot</b>	41.80 $\pm$ 3.8	40.22 $\pm$ 2.0	<b>42.97<math>\pm</math>2.0</b>	40.58 $\pm$ 4.6	37.71 $\pm$ 4.0	2.71 $\pm$ 0.4	2.78 $\pm$ 0.4	2.86 $\pm$ 0.3	25.22 $\pm$ 3.5	32.95 $\pm$ 7.4	38.78 $\pm$ 3.3
<b>chaser</b>	6.66 $\pm$ 1.0	7.51 $\pm$ 0.9	<b>8.03<math>\pm</math>0.8</b>	6.23 $\pm$ 0.9	4.02 $\pm$ 0.6	0.63 $\pm$ 0.0	0.69 $\pm$ 0.0	0.66 $\pm$ 0.0	4.73 $\pm$ 2.0	4.70 $\pm$ 1.4	4.87 $\pm$ 0.7
<b>phunder</b>	6.10 $\pm$ 1.7	7.77 $\pm$ 1.7	6.89 $\pm$ 0.5	<b>8.47<math>\pm</math>1.1</b>	6.37 $\pm$ 0.6	4.61 $\pm$ 0.3	4.74 $\pm$ 0.2	5.46 $\pm$ 0.5	5.26 $\pm$ 1.1	7.68 $\pm$ 2.1	
<b>maze</b>	6.78 $\pm$ 2.1	8.48 $\pm$ 1.4	9.28 $\pm$ 0.5	<b>9.72<math>\pm</math>0.1</b>	5.60 $\pm$ 0.2	5.17 $\pm$ 0.3	5.42 $\pm$ 0.7	5.12 $\pm$ 0.3	9.38 $\pm$ 0.3	8.52 $\pm$ 1.3	
<b>heist</b>	3.65 $\pm$ 0.5	3.70 $\pm$ 0.5	4.22 $\pm$ 1.1	<b>8.38<math>\pm</math>0.8</b>	3.25 $\pm$ 0.7	3.73 $\pm$ 0.4	3.15 $\pm$ 0.4	3.33 $\pm$ 0.7	7.62 $\pm$ 1.7	4.12 $\pm$ 1.5	
<b>Avg</b>	11.85 $\pm$ 10.8	11.23 $\pm$ 9.8	11.48 $\pm$ 10.5	11.81 $\pm$ 10.0	9.97 $\pm$ 9.7	2.63 $\pm$ 2.0	2.59 $\pm$ 1.9	2.59 $\pm$ 1.9	9.20 $\pm$ 9.0	11.14 $\pm$ 9.9	

Table 10: ProcGen ablation Test results (mean  $\pm$  std).

	Ours	Ours+Pointc.	Ours w/o Scaling	Ours+MSE	Ours+C51	Ours w/o RMS	Ours+SN (Full)	Ours+SN (Penult.)	Euc.+RMS	Euc.+HL-Gauss	Ours+Eucl.
bigfish	<b>21.56<math>\pm</math>3.5</b>	12.52 $\pm$ 3.8	15.02 $\pm$ 2.3	16.47 $\pm$ 4.6	14.77 $\pm$ 4.7	1.05 $\pm$ 0.1	1.01 $\pm$ 0.1	0.96 $\pm$ 0.1	3.71 $\pm$ 2.9	7.60 $\pm$ 3.6	19.31 $\pm$ 2.7
miner	<b>7.42<math>\pm</math>1.2</b>	7.02 $\pm$ 0.5	6.44 $\pm$ 1.4	6.23 $\pm$ 1.0	4.40 $\pm$ 1.4	1.62 $\pm$ 0.4	1.48 $\pm$ 0.3	1.33 $\pm$ 0.2	5.25 $\pm$ 2.0	4.10 $\pm$ 2.1	6.18 $\pm$ 0.7
fruitbot	<b>28.62<math>\pm</math>0.9</b>	28.04 $\pm$ 1.3	27.76 $\pm$ 1.3	28.25 $\pm$ 1.2	27.21 $\pm$ 1.3	-1.69 $\pm$ 0.2	-1.74 $\pm$ 0.3	-1.65 $\pm$ 0.3	26.82 $\pm$ 1.3	28.17 $\pm$ 0.9	27.04 $\pm$ 1.0
ninja	<b>5.57<math>\pm</math>0.6</b>	5.33 $\pm$ 0.8	4.70 $\pm$ 0.5	4.78 $\pm$ 0.2	5.35 $\pm$ 0.4	3.28 $\pm$ 0.5	3.37 $\pm$ 0.6	3.40 $\pm$ 0.2	5.13 $\pm$ 0.4	3.20 $\pm$ 1.1	4.77 $\pm$ 0.6
bossfight	<b>9.51<math>\pm</math>0.7</b>	8.60 $\pm$ 1.0	8.46 $\pm$ 0.8	9.50 $\pm$ 0.7	8.68 $\pm$ 0.9	0.78 $\pm$ 0.3	0.62 $\pm$ 0.2	0.59 $\pm$ 0.3	9.19 $\pm$ 0.8	6.10 $\pm$ 1.3	7.73 $\pm$ 0.7
coinrun	<b>8.75<math>\pm</math>0.4</b>	8.58 $\pm$ 0.4	8.75 $\pm$ 0.5	7.75 $\pm$ 0.7	8.67 $\pm$ 0.3	5.25 $\pm$ 0.6	5.35 $\pm$ 0.3	5.40 $\pm$ 0.5	7.63 $\pm$ 1.2	8.05 $\pm$ 0.2	8.38 $\pm$ 0.3
leaper	4.62 $\pm$ 1.0	3.58 $\pm$ 0.9	4.42 $\pm$ 1.1	2.47 $\pm$ 0.2	4.20 $\pm$ 1.4	3.30 $\pm$ 0.5	3.18 $\pm$ 0.5	3.27 $\pm$ 0.3	3.37 $\pm$ 1.1	3.88 $\pm$ 0.8	<b>4.67<math>\pm</math>0.7</b>
starpilot	39.85 $\pm$ 2.5	37.34 $\pm$ 2.4	39.66 $\pm$ 3.5	<b>40.14<math>\pm</math>2.8</b>	33.68 $\pm$ 4.7	2.76 $\pm$ 0.3	2.80 $\pm$ 0.3	2.58 $\pm$ 0.3	25.61 $\pm$ 2.9	32.12 $\pm$ 7.1	35.35 $\pm$ 1.7
dodgeball	8.91 $\pm$ 0.7	5.61 $\pm$ 1.1	5.28 $\pm$ 1.0	5.42 $\pm$ 1.3	5.70 $\pm$ 1.3	1.59 $\pm$ 0.3	1.54 $\pm$ 0.2	1.61 $\pm$ 0.2	2.74 $\pm$ 0.9	2.92 $\pm$ 1.3	<b>9.21<math>\pm</math>1.3</b>
chaser	6.75 $\pm$ 0.8	<b>7.08<math>\pm</math>1.2</b>	6.94 $\pm$ 0.6	5.84 $\pm$ 0.8	3.99 $\pm$ 0.5	0.65 $\pm$ 0.0	0.65 $\pm$ 0.0	0.64 $\pm$ 0.0	4.67 $\pm$ 2.1	4.24 $\pm$ 1.1	4.84 $\pm$ 0.5
jumper	5.37 $\pm$ 0.3	<b>5.73<math>\pm</math>0.2</b>	5.38 $\pm$ 0.5	5.52 $\pm$ 0.4	5.23 $\pm$ 0.6	2.50 $\pm$ 0.3	2.40 $\pm$ 0.4	2.60 $\pm$ 0.4	5.37 $\pm$ 0.1	5.03 $\pm$ 0.6	5.22 $\pm$ 0.7
maze	<b>5.58<math>\pm</math>1.5</b>	5.40 $\pm$ 0.7	5.87 $\pm$ 0.6	6.18 $\pm$ 0.8	5.22 $\pm$ 0.9	5.22 $\pm$ 0.4	5.08 $\pm$ 0.7	5.27 $\pm$ 0.5	5.55 $\pm$ 1.0	<b>6.9<math>\pm</math>0.3</b>	5.55 $\pm$ 1.4
climber	4.95 $\pm$ 1.1	5.14 $\pm$ 1.2	4.13 $\pm$ 1.3	5.79 $\pm$ 0.3	3.46 $\pm$ 0.5	2.47 $\pm$ 0.4	2.44 $\pm$ 0.3	2.39 $\pm$ 0.8	<b>6.43<math>\pm</math>0.4</b>	4.23 $\pm$ 1.3	5.48 $\pm$ 0.9
caveflyer	3.91 $\pm$ 0.2	4.05 $\pm$ 0.7	<b>5.41<math>\pm</math>0.7</b>	3.87 $\pm$ 0.3	3.62 $\pm$ 0.7	3.57 $\pm$ 0.5	3.95 $\pm$ 0.5	4.45 $\pm$ 0.5	3.99 $\pm$ 0.5	4.32 $\pm$ 0.4	4.32 $\pm$ 0.4
heist	2.43 $\pm$ 0.4	2.35 $\pm$ 0.7	2.00 $\pm$ 0.6	<b>4.23<math>\pm</math>0.7</b>	2.55 $\pm$ 0.9	2.80 $\pm$ 0.4	2.95 $\pm$ 0.4	3.27 $\pm$ 0.3	3.92 $\pm$ 0.9	2.28 $\pm$ 0.6	2.68 $\pm$ 0.4
plunder	5.08 $\pm$ 0.7	6.88 $\pm$ 1.6	6.16 $\pm$ 1.0	<b>7.59<math>\pm</math>1.3</b>	5.94 $\pm$ 0.6	4.44 $\pm$ 0.3	4.42 $\pm$ 0.3	4.45 $\pm$ 0.3	4.83 $\pm$ 0.5	4.33 $\pm$ 1.1	6.39 $\pm$ 1.3

---

## E.9 ARCHITECTURE ABLATIONS

Table 11: **Latent dimension and learned scaling  $\alpha$  ablation studies.**

Environment	$d = 32$	$d = 64$	$d = 128$	$d = 512$	$d = 64, \alpha = 0.9$	$d = 64, \alpha = 0.85$
starpilot	$40.07 \pm 4.1$	<b><math>42.49 \pm 2.6</math></b>	$41.49 \pm 2.0$	$39.07 \pm 2.9$	$39.55 \pm 4.1$	$35.61 \pm 2.7$
leaper	$4.10 \pm 1.6$	<b><math>5.13 \pm 1.0</math></b>	$4.27 \pm 1.4$	$4.35 \pm 1.6$	$4.75 \pm 1.3$	$4.90 \pm 1.0$
ninja	$5.07 \pm 0.4$	<b><math>5.68 \pm 0.4</math></b>	$5.68 \pm 0.4$	$5.40 \pm 0.3$	$5.45 \pm 0.4$	$5.68 \pm 0.9$
chaser	$6.42 \pm 0.7$	$7.27 \pm 0.9$	<b><math>7.30 \pm 0.7</math></b>	$6.63 \pm 0.6$	$6.74 \pm 0.9$	$6.40 \pm 1.2$
coinrun	$8.60 \pm 0.4$	$8.72 \pm 0.4$	$8.68 \pm 0.4$	<b><math>8.82 \pm 0.3</math></b>	$8.67 \pm 0.2$	$8.67 \pm 0.4$
bossfight	$9.23 \pm 1.2$	$9.40 \pm 0.7$	$8.94 \pm 1.0$	<b><math>9.55 \pm 0.7</math></b>	$9.00 \pm 0.7$	$9.43 \pm 0.9$
dodgeball	$9.02 \pm 1.0$	$9.41 \pm 1.2$	$9.15 \pm 1.9$	$7.16 \pm 2.3$	<b><math>9.62 \pm 1.4</math></b>	$9.07 \pm 1.5$
caveflyer	<b><math>4.33 \pm 0.9</math></b>	$4.12 \pm 0.4$	$3.98 \pm 0.5$	$4.08 \pm 0.5$	$3.93 \pm 0.6$	$3.96 \pm 0.6$
heist	$2.67 \pm 1.1$	$2.28 \pm 1.0$	$2.42 \pm 0.5$	$2.60 \pm 0.6$	<b><math>2.73 \pm 0.7</math></b>	$2.20 \pm 0.4$
fruitbot	$27.65 \pm 1.8$	$28.28 \pm 0.9$	<b><math>28.81 \pm 0.8</math></b>	$28.75 \pm 0.8$	$27.87 \pm 0.5$	$28.01 \pm 1.5$
maze	$5.68 \pm 0.4$	$5.17 \pm 0.8$	<b><math>5.70 \pm 1.2</math></b>	$5.57 \pm 0.4$	$5.40 \pm 0.7$	$5.48 \pm 0.7$
miner	<b><math>7.76 \pm 0.6</math></b>	$7.21 \pm 0.7$	$6.63 \pm 0.9$	$6.46 \pm 0.7$	$7.11 \pm 1.1$	$7.44 \pm 0.4$
climber	$5.10 \pm 0.9$	$5.86 \pm 1.2$	<b><math>6.54 \pm 1.0</math></b>	$6.42 \pm 1.1$	$6.20 \pm 0.9$	$5.70 \pm 0.6$
jumper	$5.15 \pm 0.4$	$5.30 \pm 0.4$	$5.22 \pm 0.6$	$5.90 \pm 0.4$	$5.32 \pm 0.7$	<b><math>5.98 \pm 0.4</math></b>
plunder	$6.40 \pm 1.0$	$5.82 \pm 1.6$	$6.17 \pm 1.2$	$5.85 \pm 0.7$	<b><math>6.71 \pm 0.6</math></b>	$6.01 \pm 0.7$
bigfish	$20.77 \pm 2.0$	$20.01 \pm 4.8$	<b><math>20.96 \pm 2.4</math></b>	$19.84 \pm 4.2$	$19.55 \pm 2.9$	$20.89 \pm 3.3$
<b>IQM (normalized)</b>	0.38	0.41	<b>0.42</b>	0.39	0.40	0.41